Inorganic Chemistry

Article

pubs.acs.org/IC

Generation of a High-Valent Iron Imido Corrolazine Complex and NR Group Transfer Reactivity

Pannee Leeladee,[†] Guy N. L. Jameson,*[,‡] Maxime A. Siegler,[†] Devesh Kumar,[⊥] Sam P. de Visser,*[,∥] and David P. Goldberg*[,†]

[†]Department of Chemistry, The Johns Hopkins University, 3400 North Charles Street, Baltimore, Maryland 21218, United States

[‡]Department of Chemistry and MacDiarmid Institute for Advanced Materials and Nanotechnology, University of Otago, P.O. Box 56, Dunedin 9054, New Zealand

[⊥]Department of Applied Physics, Babasaheb Bhimrao Ambedkar University, Vidya Vihar, Rai Bareilly Road, Lucknow 226 025, India

[∥]Manchester Institute of Biotechnology and School of Chemical Engineering and Analytical Science, The University of Manchester, 131 Princess Street, Manchester M1 7DN, United Kingdom

Supporting Information

ABSTRACT: The generation of a new high-valent iron terminal imido complex prepared with a corrolazine macrocycle is reported. The reaction of $[Fe^{III}(TBP_8Cz)]$ (TBP_8Cz = octakis(4-*tert*-butylphenyl)corrolazinato) with the commercially available chloramine-T (Na^+TsNCl^-) leads to oxidative N-tosyl transfer to afford $[Fe^{IV}(TBP_8Cz^{+\bullet})(NTs)]$ in dichloromethane/acetonitrile at room temperature. This complex was characterized by UV−vis, Mössbauer (δ = −0.05 mm s^{-1}, ΔE_Q = 2.94 mm s^{-1}), and EPR (X-band (15 K), g = 2.10, 2.00) spectroscopies, and together with reactivity patterns and DFT calculations has been established as an iron(IV) species antiferromagnetically coupled with a Cz-π-cation-radical (S_{total} = $^1/_2$ ground state). Reactivity studies with triphenylphosphine as substrate show that $[Fe^{IV}(TBP_8Cz^{+\bullet})(NTs)]$ is an efficient NTs transfer agent, affording the phospharane product $Ph_3P{=}NTs$ under both stoichiometric and catalytic conditions. Kinetic analysis of this reaction supports a bimolecular NTs transfer mechanism with rate constant of 70(15) M^{-1} s^{-1}. These data indicate that $[Fe^{IV}(TBP_8Cz^{+\bullet})(NTs)]$ reacts about 100 times faster than analogous Mn terminal arylimido corrole analogues. It was found that two products crystallize from the same reaction mixture of $Fe^{III}(TBP_8Cz)$ + chloramine-T + PPh_3, $[Fe^{IV}(TBP_8Cz)(NPPh_3)]$ and $[Fe^{III}(TBP_8Cz)(OPPh_3)]$, which were definitively characterized by X-ray crystallography. The sequential production of $Ph_3P{=}NTs$, $Ph_3P{=}NH$, and $Ph_3P{=}O$ was observed by ^{31}P NMR spectroscopy and led to a proposed mechanism that accounts for all of the observed products. The latter Fe^{III} complex was then rationally synthesized and structurally characterized from $Fe^{III}(TBP_8Cz)$ and $OPPh_3$, providing an important benchmark compound for spectroscopic studies. A combination of Mössbauer and EPR spectroscopies led to the characterization of both intermediate spin (S = $^3/_2$) and low spin (S = $^1/_2$) Fe^{III} corrolazines, as well as a formally Fe^{IV} corrolazine which may also be described by its valence tautomer $Fe^{III}(Cz^{+\bullet})$.

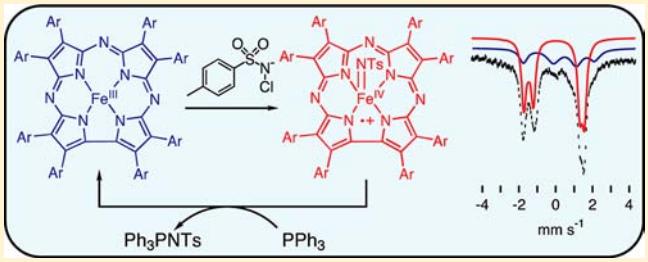

INTRODUCTION

Iron−nitrogen multiply bonded complexes have been implicated in biological systems and industrial processes. For instance, in the Haber−Bosch process, iron-bound surface nitrides have been postulated as the reactive intermediates responsible for ammonia production.[1,2] The iron-containing metalloenzyme nitrogenase likely relies upon one or more multiply bonded Fe−N intermediates during the dinitrogen reduction process.[3−5] An Fe=NR porphyrin species was suggested as the reactive intermediate for reactions involving NR insertion into C−H bonds by the heme enzyme Cytochrome P450-LM 3,4.[6] In analogy to this chemistry, much effort has gone into accessing transient Fe−N(R) multiply bonded species as potent catalysts for C−H activation and functionalization.[7−11] There is great interest in preparing metal-nitrido and metal-imido complexes, including iron-based systems, for similar potential applications in atom or group transfer processes.[12−17]

The synthesis of mid- to late-transition metal-imido complexes has been quite challenging. The stability of these compounds depends on their geometry, the oxidation state of the metal, and the nature of the ancillary ligands. In particular, 5- or 6-coordinate Fe-imido complexes are usually considered highly unstable, making it difficult to generate and/or characterize such species. It can be seen from qualitative d-orbital splitting diagrams that these high coordination number iron complexes would normally have filled, or partially filled,

Received: February 2, 2013
Published: March 25, 2013

Chart 1. Representative Examples of Multiply-Bonded, Terminal-Imido/Nitrene Fe and Mn Complexes (Ad = adamantyl; Ts = tosyl; Mes = mesityl)

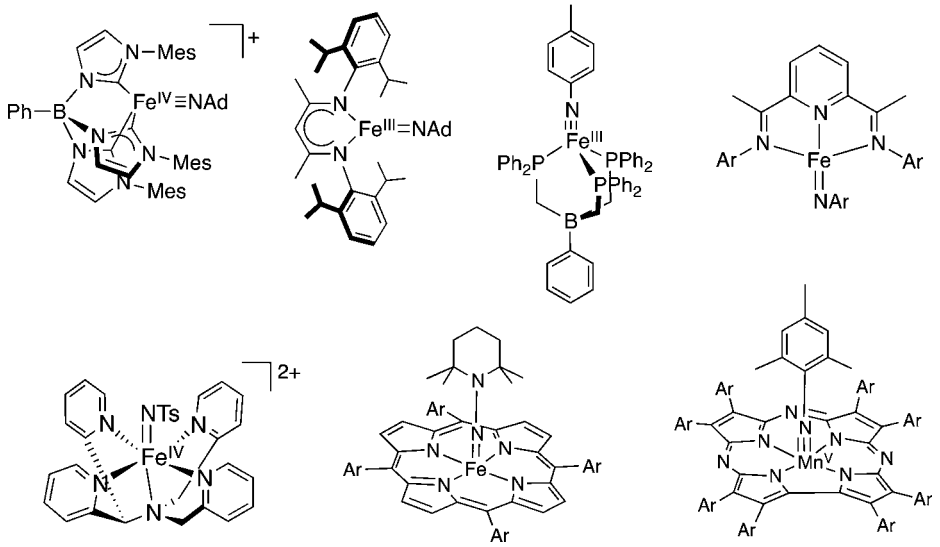

dπ-pπ antibonding orbitals with respect to the Fe−N interaction. The Fe ion needs to be in an unusually high oxidation state, e.g., Fe(6+), to avoid this destabilizing influence,[18] and iron compounds in relatively low oxidation states, e.g. Fe(2+), Fe(3+), are destabilized due to the population of the antibonding dπ(Fe)−pπ(N) orbitals.[9,10,17,19] To our knowledge, there is only one example of an Fe(NR) complex with a coordination number ≥5 that has been crystallographically characterized, and this complex is an iron porphyrin derivative.[20] Interestingly, this complex was formulated as a high-spin Fe^{II}-nitrene compound, as indicated by Mössbauer spectroscopy. In addition, a 6-coordinate, nonheme Fe^{IV}-imido complex supported by a tetrapyridylamine ligand was described, but this complex could not be characterized by X-ray crystallography (Chart 1).[21]

An alternative, elegant strategy to prepare stable Fe terminal imido complexes is to construct them from compounds with low coordination number (Chart 1). Peters and co-workers have shown that triply bonded Fe^{II}-, Fe^{III}-, and Fe^{IV}-imido complexes can be stabilized in pseudotetrahedral coordination environments by sterically encumbered tris(phosphino)borane, tris(phosphino)borate, and bis(phosphine)pyrazolyl ligands.[22−26] Similarly, Smith and co-workers introduced strong field, bulky tris(carbene)borate ligands to stabilize Fe^{III}- and Fe^{IV}-imido complexes with 3-fold symmetry.[27] Iron-imide complexes with redox-active bis(imino)pyridine (BIP) ligands have been constructed from distorted square planar geometries,[28,29] although the assignment of the iron oxidation states in these compounds is not straightforward.[28] Highly unsaturated, three-coordinate iron(III) terminal imido complexes have also been prepared with either bulky bidentate, β-diketiminate ligands,[30,31] or bidentate, dipyrromethene-based systems.[8] In all of these cases it seems that the steric encumbrance of the surrounding ligands is essential to engender the low-coordinate environments that stabilize iron-imido species.

Our group has focused on the stabilization and characterization of high-valent manganese and iron complexes with multiply bonded terminal ligands encapsulated in the heme-like corrolazine (Cz) platform. The strongly donating and oxidatively resistant Cz macrocycle has allowed for the isolation and X-ray crystallographic characterization of a high-valent Mn^{V}-imido complex, [Mn^{V}(TBP$_8$Cz)(NMes)] (Mes = 2,4,6-trimethylphenyl; TBP$_8$Cz = octakis(4-*tert*-butylphenyl)-corrolazinato) (Chart 1).[32] The related corrole (Cor) complex, [Mn^{V}(tpfc)(NMes)] (tpfc = *meso*-tris(pentafluorophenyl)-corrole), was also isolated and fully characterized, including an X-ray structure determination.[33] Isoelectronic Mn^{V} terminal oxo complexes have also been generated with Cz and Cor supporting ligands, and the first example of this class, Mn^{V}(O)(TBP$_8$Cz), was isolable and stable as a solid at room temperature.[34−38] In these cases the paradigm does not involve enforcing low-coordinate environments at the metal center; rather the Cz and Cor ligands are designed to provide strong, in-plane σ donation that helps stabilize metal ions in high-valent states, depopulating the key, dπ−pπ antibonding orbitals involved in terminal imido/oxo ligation.

The synthesis of these rare, manganese-imido/oxo complexes suggested to us that the Cz scaffold might support the preparation of analogous high-valent, iron-imido complexes. Indeed, we had already described the generation, low-temperature stabilization, and C−H activation chemistry of a high-valent, iron-oxo corrolazine π-cation-radical (Fe^{IV}(O)-(TBP$_8$Cz$^{+\bullet}$)), equivalent to the compound-I intermediate in heme enzymes.[39,40] It has been shown that Fe^{III} corroles can catalyze aziridinations using PhINTs as the nitrogen source, and a high-valent Fe-imido species was postulated as the reactive intermediate.[41] In the same study, an Fe^{IV} corrole was also found to be a potent catalyst for aziridinations when PhINTs was replaced with chloramine-T (Na^{+}TsNCl^{-}) as the nitrogen source. However, no direct spectroscopic evidence for the existence of high-valent Fe-imido corroles in this study, or any other, has thus far been obtained.

Herein, we report the generation of a high-valent iron-imido corrolazine, (TBP$_8$Cz$^{+\bullet}$)Fe^{IV}(NTs), and its characterization through a combination of UV−vis, EPR, and Mössbauer spectroscopies. Density functional theory (DFT) calculations were performed to support and analyze the electronic structure assignment, and simulate the Mössbauer parameters for the high-valent iron-imido complex. This complex is a rare example of a metastable Fe-imido porphyrinoid compound, and the first example of such a species housed in a corrole-type macrocycle.

dx.doi.org/10.1021/ic400280x | *Inorg. Chem.* 2013, 52, 4668−4682

It is shown that this compound is capable of NR group transfer to PPh_3 to give the $TsN{=}PPh_3$ product with concomitant two-electron reduction of the iron-imido complex. Kinetic studies show that the reactivity of the Fe=NTs complex is dramatically enhanced over Mn=NAr corroles. However, $(TBP_8Cz^{+\bullet})Fe^{IV}(NTs)$ is, in general, significantly more stable (and less reactive) than expected for a multiply bonded, iron-imido species. Crystal structures were determined for the PPh_3-derived products $[Fe^{IV}(TBP_8Cz)(NPPh_3)]$ and $[Fe^{III}(TBP_8Cz)(OPPh_3)]$, and these structures have aided in our understanding of the mechanism of NR transfer and subsequent product transformations. Combined EPR and Mössbauer studies on the series of iron complexes described here provide insights into the oxidation state assignments and ligand noninnocence for such compounds.

EXPERIMENTAL DETAILS

All reactions were performed using dry solvents and standard Schlenk or drybox techniques at room temperature unless otherwise noted. The complex $[Fe^{III}(TBP_8Cz)]$ (**1**)[42] and metal-free corrolazine TBP_8CzH_3[43] were synthesized as reported previously. The $^{57}FeCl_2$ was prepared according to a published procedure.[44] Dichloromethane and acetonitrile were purified via a Pure-Solv solvent purification system from Innovative Technologies, Inc. Deuterated solvents for NMR samples were purchased from Cambridge Isotope Laboratories, Inc. Chloramine-T trihydrate ($Na^+TsNCl^-{\cdot}3H_2O$) was purchased from Sigma-Aldrich and used as received. Triphenylphosphine (PPh_3) was received from Sigma-Aldrich and recrystallized from diethyl ether. Triphenylphosphine oxide (Ph_3PO) was purchased from Sigma-Aldrich and recrystallized from ethanol. Authentic samples of (*N*-tosylimino)triphenylphosphorane (Ph_3PNTs) and Ph_3PNH were synthesized according to published methods.[45,46]

Instrumentation. UV−vis spectroscopy was performed on a Varian Cary 50 Bio spectrophotometer. Kinetic experiments were run on a Hewlett-Packard 8542 diode-array spectrophotometer equipped with HPChemstation software. Electron paramagnetic resonance (EPR) spectra were obtained on a Bruker EMX EPR spectrometer controlled with a Bruker ER 041 X G microwave bridge at 15 K, and equipped with a continuous-flow liquid helium cryostat (ESR900) coupled to a TC503 temperature controller made by Oxford Instruments, Inc. ^1H NMR and ^{31}P NMR spectra were recorded on a Bruker Avance 400 MHz FT-NMR spectrometer. Chemical shifts were referenced to the residual solvent peaks for ^1H NMR and to the H_3PO_4 peak for ^{31}P NMR. Electrospray ionization mass spectra (ESI-MS) were collected on a Thermo Finnigan LCQ Duo ion-trap mass spectrometer fitted with an electrospray ionization source in positive ion mode. Samples were infused into the instrument at a rate of 25 μL/min using a syringe pump via a silica capillary line. The spray voltage was set at 5 kV, and the capillary temperature was held at 250 °C. ^{57}Fe Mössbauer spectra were recorded on a Mössbauer spectrometer from SEE Co. (Science Engineering & Education Co., MN) equipped with a closed cycle refrigerator system from Janis Research Co. and SHI (Sumitomo Heavy Industries Ltd.). Data were collected in constant acceleration mode in transmission geometry. The zero velocity of the Mössbauer spectra refers to the centroid of the room temperature spectrum of a 25 μm metallic iron foil. Analysis of the spectra was conducted using the WMOSS program (SEE Co, formerly WEB Research Co. Edina, MN). Magnetic spectra were fitted using the spin Hamiltonian:

$$H = D\left[\hat{S}_z^2 - \frac{1}{3}S(S+1)\right] + E(\hat{S}_x^2 - \hat{S}_y^2) + \beta\hat{S}\cdot g\cdot\hat{B} \quad (1)$$

Computational Calculations and Spectroscopic Parameter Determination. All calculations were done using previously described methods[47] with density functional theory at the unrestricted hybrid density functional level UB3LYP[48,49] as implemented in the *Jaguar 7.9* and *Gaussian-03* program packages.[50,51] All geometries described here were the result of a full optimization without geometric constraints, and the local minima were ascertained with an analytical frequency calculation that established real frequencies only. These optimizations and frequencies were done with an LACVP basis set on Fe that includes a core potential and a 6-31G basis set on the rest of the atoms: basis set B1.[52] This basis set was shown to give adequate structures for the investigation of a potential energy profile of a chemical reaction by an iron(IV)-oxo species.[53] To improve the energetics we did single point calculations using a triple-ζ quality LACV3P+ basis set on Fe (with core potential) and 6-311+G* on the rest of the atoms: basis set B2. Energies reported in here are taken from the UB3LYP/B2 results and are corrected for zero-point energies at UB3LYP/B1. Free energies use UB3LYP/B2 energies and UB3LYP/B1 zero-point energies, thermal and entropic corrections. We also did single point calculations in Jaguar using the Polarized Continuum Model using a dielectric constant of $\varepsilon = 5.708$ and probe radius of 2.722 Å.

Spectroscopic parameters (Mössbauer and EPR parameters) were obtained from single point calculations on the optimized geometries using the ORCA program package.[54] These calculations used the B3LYP method in combination with the CP(PPP) basis set on Fe coupled to a TZVP basis set on the rest of the atoms.[55] The electric field gradients V_i ($i = x, y,$ or z) were used to calculate the quadrupole splitting (ΔE_Q) using eqs 2 and 3 with e the elementary charge of a proton/electron, Q the nuclear quadrupole moment, $Q(^{57}Fe) = 0.16$ barn, and η the asymmetry parameter of the nuclear quadrupole tensor.[56]

$$\Delta E_Q = \frac{1}{2}eQ\cdot V_z\cdot\sqrt{1+\frac{1}{3}\eta^2} \quad (2)$$

$$\eta = (V_x - V_y)/V_z \quad (3)$$

The isomer shift δ was calculated from the spin density at the iron nucleus $\rho_0(Fe)$ using previously determined fit-parameters in ORCA.[57] The magnetic hyperfine parameters, A_i ($i = x, y,$ or z), were obtained using the scalar relativistic zero-order regular approximation (ZORA) at the B3LYP level of theory. These methods were shown to reproduce well experimentally determined Mössbauer and EPR parameters of transition metal complexes.

Generation of $[Fe^{IV}(TBP_8Cz^{+\bullet})(NTs)]$ (2) in Situ. To a solution of $[Fe^{III}(TBP_8Cz)]$ (16 μM) in CH_2Cl_2 was added $Na^+TsNCl^-{\cdot}3H_2O$ (1 equiv dissolved in CH_3CN). A color change of the solution from green to brown was noted. The reaction was monitored by UV−vis spectroscopy, revealing isosbestic conversion from the spectrum for **1** to that of the new brown species $[Fe^{IV}(TBP_8Cz^{+\bullet})(NTs)]$ (**2**) (λ_{max} = 395, $\varepsilon = 4.3\times10^4\ M^{-1}\ cm^{-1}$). The spectrum for **2** is stable for at least 2 h at room temperature. An EPR sample was prepared as follows: to a solution of $[Fe^{III}(TBP_8Cz)]$ (2.0 mM) in toluene (300 μL) was added chloramine-T (1 equiv dissolved in CH_3CN) to give a final concentration of 1.5 mM of the iron complex. A color change from green to brown was observed. The reaction mixture was then transferred to a Wilmad quartz EPR tube (3 mm i.d.), and the sample was frozen and stored at 77 K.

Precipitation of Solid $[Fe^{IV}(TBP_8Cz^{+\bullet})(NTs)]$ (2). To an amount of $[Fe^{III}(TBP_8Cz)]$ (20.6 mg, 14.6 μmol) in CH_2Cl_2 (1.00 mL) was added $Na^+TsNCl^-{\cdot}3H_2O$ (6.2 mg, 22 μmol, 1.5 equiv) dissolved in CH_3CN (0.40 mL). The reaction mixture was stirred for 30 min, and the color change from green to brown was observed. An amount of CH_3CN was added until a solid precipitate had formed in the reaction mixture. The resulting solid was filtered, isolated on filter paper, and washed with CH_3CN to afford a dark brown-green solid (8.0 mg).

Kinetics of NR Group Transfer to Triphenyl Phosphine. In a custom-made 100-mL round-bottom flask adapted with a 1-cm path-length side arm UV−vis cell was prepared a solution of $[Fe^{IV}(TBP_8Cz^{+\bullet})(NTs)]$ (**2**) by addition of $Na^+TsNCl^-{\cdot}3H_2O$ (100 μL of an 0.8 mM stock solution in CH_3CN, 1 equiv) to a solution of **1** (16 μM) dissolved in CH_2Cl_2 (5 mL). The cell was placed in the spectrophotometer, and a 400 nm long-pass filter was placed between the spectrophotometer light source and the sample solution in order to

dx.doi.org/10.1021/ic400280x | Inorg. Chem. 2013, 52, 4668−4682

avoid any potential photodegradation of iron corrolazine. After complete conversion of **1** to **2** was noted by UV−vis, excess PPh_3 (30−75 equiv dissolved in CH_2Cl_2) was added to start the reaction, and an immediate color change from brown to green was noted, indicating the recovery of the starting material **1**. The time-course of the reaction was monitored by UV−vis and showed a smooth conversion of **2** to **1** over a 100−200 s period depending on the concentration of PPh_3. The pseudo-first-order rate constants, k_{obs}'s, for this reaction were obtained by nonlinear least-squares fitting of the plots of absorbance (Abs) at 440 nm versus time (t) to the following equation:

$$Abs_t = Abs_f - (Abs_f - Abs_0)e^{-k_{obs}t} \quad (4)$$

Here, Abs_f = final absorbance and Abs_0 = initial absorbance. The reaction was repeated over a range of substrate concentrations, and a plot of k_{obs} versus substrate concentration was found to be linear. The second-order rate constant (k) was obtained from the slope of the best-fit line to this plot.

Monitoring of NR Group Transfer by ^{31}P NMR Spectroscopy. To a solution of **1** (12−15 mM) in CD_2Cl_2 was added $Na^+TsNCl^-\cdot 3H_2O$ (1−3 equiv dissolved in CD_3CN). A color change from green to brown was noted, consistent with formation of **2**. An aliquot of the reaction mixture was checked by UV−vis spectroscopy to ensure the complete formation of **2**. Excess PPh_3 (5−10 equiv dissolved in CD_2Cl_2) was added, causing an immediate color change from brown to green. An aliquot of the reaction mixture was removed and analyzed by UV−vis spectroscopy, revealing the return of **1**. The solution was then transferred to an NMR tube, and the reaction was monitored by ^{31}P NMR over 14 d.

Synthesis of [Fe(TBP$_8$Cz)(NPPh$_3$)] (3). A reaction of **2** with PPh_3 substrate was performed as described above for ^{31}P NMR experiments, and then the reaction mixture was allowed to stand in an NMR tube under ambient conditions. Good quality single crystals appeared after 2 weeks. A crystal was selected for X-ray structure determination and revealed the structure for [Fe(TBP$_8$Cz)(NPPh$_3$)] (**3**). ESI-MS, EPR, and Mössbauer data indicated that the bulk material of these crystals was contaminated with a small amount of [Fe(TBP$_8$Cz)(OPPh$_3$)], and a separate X-ray structure determination of a second crystal confirmed the presence of this complex, whose structure was solved as [Fe(TBP$_8$Cz)(OPPh$_3$)] (**4a**).

Synthesis of [Fe(TBP$_8$Cz)(OPPh$_3$)] (4b). To a solution of **1** (9.8 mg, 6.9 μmol) in CH_2Cl_2 (400 μL) was added Ph_3PO (5 equiv in 100 μL of CH_2Cl_2). An amount of CH_3CN (100 μL) was added, and good quality single crystals (black blocks) (8 mg, 68%) were obtained by slow evaporation of this mixture for one week. UV−vis (CH_2Cl_2): λ_{max} = 439, 607, 732 nm. ESI-MS (m/z): isotopic cluster centered at 1689.7 (M^+). ^{1}H NMR (CD_2Cl_2): δ (ppm) 13.05 (br), 11.26 (br), 9.95 (br), 7.47 (br), 2.00, 1.82, 1.66, 1.57, 1.26, 0.88. ^{31}P NMR (CD_2Cl_2): δ (ppm) 27.4. Anal. Calcd for $C_{114}H_{119}FeN_7OP$: C, 81.02: H, 7.10; N, 5.80. Found: C, 81.18; H, 7.03; N, 5.78.

X-ray Crystallography. All reflection intensities were measured at 110(2) K using a KM4/Xcalibur (detector: Sapphire3) with enhanced graphite-monochromated Mo Kα radiation (λ = 0.710 73 Å) under the program CrysAlisPro (Version 1.171.33.55 or 1.171.35.11, Agilent Technologies, 2010/2011). The temperature of the data collection was controlled using the system Cryojet (manufactured by Oxford Instruments). The program CrysAlisPro (Version 1.171.33.55 or 1.171.35.11, Agilent Technologies, 2010/2011) was used to refine the cell dimensions and data reduction. The structure was solved with the program SHELXS-97 and was refined on F^2 with SHELXL-97. Analytical numeric absorption corrections based on a multifaceted crystal model were applied using CrysAlisPro (Version 1.171.33.55 or 1.171.35.11, Agilent Technologies, 2010/2011). The H-atoms were placed at calculated positions using the instructions AFIX 23, AFIX 43, or AFIX 137 with isotropic displacement parameters having values 1.2 or 1.5 times U_{eq} of the attached C atoms.

The asymmetric unit of **3**, **4a**, and **4b** contains one Fe complex, and some lattice dichloromethane and acetonitrile solvent molecules. All structures are partly disordered. The t-butyl group C73→C76 of one aryl group is disordered over two orientations, and the occupancy factor for the major component refines to 0.876(5) for **3**, 0.870(5) for **4a**, and 0.895(4) for **4b**. In the structure of **3**, disorder was modeled for the four crystallographically independent dichloromethane molecules, and the occupancy factors for the major components are 0.831(4), 0.880(2), 0.695(5), and 0.529(8). In the structures of **4a** and **4b**, free variables for the major occupancy factors of one disordered CH_2Cl_2 and one ordered CH_3CN solvent molecules were used in the final refinement. Their refined values are 0.753(4), 0.131(3), and 0.902(8) for **4a**, and 0.792(4), 0.113(3), and 0.923(8) for **4b**. Other solvent molecules were found in the crystal lattice but were significantly more disordered, and therefore, their contributions were taken out by using the program SQUEEZE (Spek, 2003) for the final refinement.

Data for **3** follow: fw = 2068.75, black block, 0.34 × 0.31 × 0.26 mm^3, monoclinic, $P2_1/c$ (No. 14), a = 17.2124(2) Å, b = 33.4786(5) Å, c = 19.9855(2) Å, β = 102.6307(12)°, V = 11237.9(2) Å^3, Z = 4, D_x = 1.223 g cm^{-3}, μ = 0.390 mm^{-1}, abs corr range 0.894−0.923. There were 65 453 reflections measured up to a resolution of $(\sin\theta/\lambda)_{max}$ = 0.59 Å^{-1}. There were 19 786 unique reflections (R_{int} = 0.0377), of which 13 559 were observed [$I > 2\sigma(I)$]. There were 1354 parameters refined using 180 restraints. R1/wR2 [$I > 2\sigma(I)$]: 0.0666/0.1901. R1/wR2 [all reflns]: 0.0961/0.2026. S = 1.069. Residual electron density found between −0.93 and 0.78 e Å^{-3}.

Data for **4a** follow (asterisk indicates exclusion of the contribution of the unresolved residual electron density): *fw = 1802.09, *black block, 0.62 × 0.51 × 0.30 mm^3, monoclinic, $P2_1/c$ (No. 14), a = 17.2614(8) Å, b = 33.4143(11) Å, c = 19.9714(8) Å, β = 102.610(4)°, V = 11241.2(8) Å^3, Z = 4, D_x = 1.065 g cm^{-3}, *μ = 0.239 mm^{-1}, *abs corr range 0.899−0.941. *There were 59 539 reflections measured up to a resolution of $(\sin\theta/\lambda)_{max}$ = 0.59 Å^{-1}. There were 19 795 unique reflections (R_{int} = 0.0449), of which 15 006 were observed [$I > 2\sigma(I)$]. There were 1221 parameters refined using 63 restraints. R1/wR2 [$I > 2\sigma(I)$]: 0.0605/0.1733. R1/wR2 [all reflns]: 0.0759/0.1822. S = 1.069. Residual electron density found between −0.47 and 0.66 e Å^{-3}.

Data for **4b** follow: *fw = 1804.71, *black block, 0.35 × 0.24 × 0.20 mm^3, monoclinic, $P2_1/c$ (No. 14), a = 17.2502(2) Å, b = 33.4217(5) Å, c = 19.9821(2) Å, β = 102.7119(12)°, V = 11237.9(2) Å^3, Z = 4, D_x = 1.067 g cm^{-3}, *μ = 0.240 mm^{-1}, *abs corr range 0.900−0.937. There were *64 199 reflections measured up to a resolution of $(\sin\theta/\lambda)_{max}$ = 0.59 Å^{-1}. There were 19 786 unique reflections (R_{int} = 0.0375), of which 14 933 were observed [$I > 2\sigma(I)$]. There were 1221 parameters refined using 63 restraints. R1/wR2 [$I > 2\sigma(I)$]: 0.0611/0.1662. R1/wR2 [all reflns]: 0.0791/0.1750. S = 1.073. Residual electron density found between −0.40 and 0.66 e Å^{-3}.

Synthesis of [^{57}Fe^{III}(TBP$_8$Cz)]. The metal-free corrolazine TBP_8CzH_3 (62 mg, 0.046 mmol) was combined with $^{57}FeCl_2$ (29 mg, 0.23 mmol) in dimethylformamide (10 mL) and heated at reflux for 2 h. After removing the solvent *in vacuo*, the crude product was purified by flash column chromatography (CH_2Cl_2/MeOH 99:1 v/v; silica gel) to obtain [^{57}Fe^{III}(TBP$_8$Cz)] as a dark-green solid (51 mg, 79%). UV−vis (CH_2Cl_2): λ_{max} = 441, 610, 746 nm.

Samples for Mössbauer Studies. The ^{57}Fe-labeled complexes [^{57}Fe^{III}(TBP$_8$Cz)] and [^{57}Fe^{III}(TBP$_8$Cz)(NPPh$_3$)] were used for Mössbauer measurements. An isotopically labeled sample of **3** ([^{57}Fe^{III}(TBP$_8$Cz)(NPPh$_3$)]) was synthesized from [^{57}Fe^{III}(TBP$_8$Cz)] starting material. In the case of [Fe^{III}(TBP$_8$Cz)(OPPh$_3$)] (**4b**), Mössbauer data were collected on samples that were not enriched in ^{57}Fe. Samples were either measured as solid-state samples (~10 mg) or as frozen solutions (~400 μL) in toluene or pyridine in custom-made Teflon sample holders.

RESULTS AND DISCUSSION

Synthesis and Characterization of a High-Valent Iron Imido Corrolazine Complex. A variety of discrete metal-imido complexes have been synthesized by the reaction of the appropriate metal precursors and alkyl- or aryl-azides.[9,32,33,58−61] This strategy was used to synthesize the Mn^V-imido complex [Mn^V(TBP$_8$Cz)NMes], in which the Mn^{III}

dx.doi.org/10.1021/ic400280x | Inorg. Chem. 2013, 52, 4668−4682

precursor [$Mn^{III}(TBP_8Cz)$] was reacted with mesityl azide (2,4,6-$(CH_3)_3C_6H_2N_3$) at elevated temperature.[32] Corrole analogues [Mn(tpfc)NAr] (Ar = 2,4,6-$(CH_3)_3C_6H_2$, 2,4,6-$Cl_3C_6H_2$) have been similarly prepared.[33] Our initial efforts to gain access to a high-valent Fe-imido corrolazine followed the same methodology. Attempts were made to react the previously synthesized Fe^{III} complex [$Fe^{III}(TBP_8Cz)$] with both alkyl- and aryl-azides. For example, [$Fe^{III}(TBP_8Cz)$] was stirred with 50 equiv of mesityl azide in toluene for 24 h, but even at elevated temperature (90 °C) no evidence of reaction in the form of a color change, UV−vis spectroscopic conversion, or TLC change was noted. The azides AdN_3 (Ad = adamantyl), PhN_3, and Me_3SiN_3 were examined under similar conditions, but none led to any noticeable reaction with the Fe^{III} corrolazine. We speculated that the coordination of the azide reagents, or the triplet nitrene that potentially forms upon thermal activation of the azides,[61] was not occurring because even small changes in the UV−vis spectrum of [$Fe^{III}(TBP_8Cz)$] were not observed. The failure of the azide reagents to react with [$Fe^{III}(TBP_8Cz)$] prompted us to examine alternative NR group transfer reagents.

The inexpensive, commercially available reagent chloramine-T ($Na^+TsNCl^-\cdot 3H_2O$) was shown to be a good NTs-transfer agent in catalytic aziridinations involving Fe corrole [(Fe^{IV}(tpfc)],[41] and both chloramine-T and bromamine-T have been used as a nitrene source in metal-catalyzed C−H insertions.[41,62−65] Addition of a stock solution of chloramine-T in CH_3CN to [$Fe^{III}(TBP_8Cz)$] dissolved in CH_2Cl_2 at room temperature led to the conversion of green [$Fe^{III}(TBP_8Cz)$] (λ_{max} = 440, 611, 747 nm) to a new, brown species with λ_{max} = 395 nm (Figure 1). Isosbestic points are observed at 392, 490,

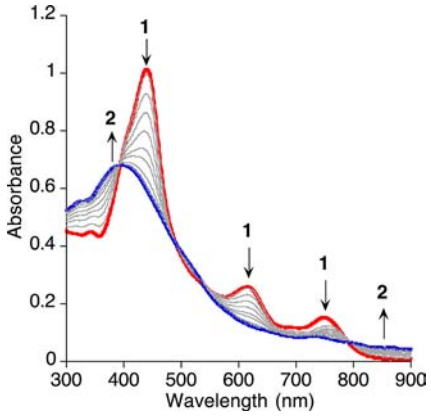

Figure 1. UV−vis spectral change upon addition of chloramine-T trihydrate (0−1.0 equiv) to [$Fe^{III}(TBP_8Cz)$] at 23 °C in CH_2Cl_2/CH_3CN.

538, and 792 nm. The new species with λ_{max} = 395 nm appears surprisingly stable for more than 2 h at room temperature as monitored by UV−vis. The changes in the UV−vis following addition of chloramine-T are similar to those observed for the reaction of [$Fe^{III}(TBP_8Cz)$] and pentafluoroiodosylbenzene to give the high-valent iron-oxo complex [$Fe^{IV}(TBP_8Cz^{+\bullet})(O)$], although in this case the iron-oxo product is thermally unstable and had to be observed at low temperature (−78 °C) (Figure 2). The UV−vis data are consistent with the formation of the expected product, [$Fe^{IV}(TBP_8Cz^{+\bullet})(NTs)$] (**2**), in which the tosylimido group replaces the terminal oxo ligand of [$Fe^{IV}(TBP_8Cz^{+\bullet})(O)$] and the Fe^{III} complex is oxidized by

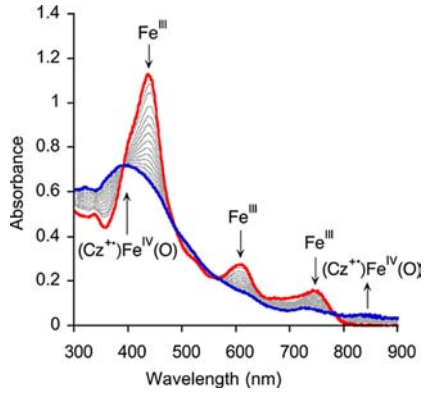

Figure 2. UV−vis spectral change upon addition of pentafluoroiodosylbenzene (PFIB) to [$Fe^{III}(TBP_8Cz)$] at −78 °C in CH_2Cl_2/CH_3OH.

two electrons, as shown in Scheme 1. The stoichiometry of the reaction was determined by titration of chloramine-T followed by monitoring by UV−vis spectroscopy, as shown in Figures 1 and S1. Addition of chloramine-T in 0.1 equiv increments results in isosbestic conversion of the Fe^{III} complex up to a total of 1 equiv, at which point a loss of isosbestic behavior is observed together with a decrease at 395 nm corresponding to the oxidized product. This spectral titration confirms that chloramine-T and [$Fe^{III}(TBP_8Cz)$] (**1**) react in a ratio of 1:1 to form [$Fe^{IV}(TBP_8Cz^{+\bullet})(NTs)$] (**2**). The imido complex **2** is thus remarkably stable in solution at room temperature, and this stability is likely a consequence of the previously established ability of the corrolazine platform to stabilize high-valent, multiply bonded terminal oxo and terminal imido complexes.

Several attempts were made to grow single crystals of the product from chloramine-T for X-ray structure determination, but thus far these efforts have remained unsuccessful. However, the complex can be isolated as a solid by solvent precipitation. Relatively concentrated solutions of [$Fe^{IV}(TBP_8Cz^{+\bullet})(NTs)$] (10 mM) can be generated in CH_2Cl_2 from [$Fe^{III}(TBP_8Cz)$] and chloramine-T, and the resulting Fe═NTs product is then precipitated from the reaction mixture by the addition of excess CH_3CN. Formation of a brown-green solid and a brown solution results, and the solid is then isolated by filtration. This solid exhibited similar UV−vis and other spectroscopic properties as seen for a sample of [$Fe^{IV}(TBP_8Cz^{+\bullet})(NTs)$] freshly generated in CH_2Cl_2, indicating that the precipitated material contains the [$Fe^{IV}(TBP_8Cz^{+\bullet})(NTs)$] complex prepared in situ. However, Mössbauer spectroscopic measurements show that this solid cannot be isolated in pure form, and contains up to ∼25% of the starting Fe^{III} complex (vide infra). Autoreduction of the iron-imido complex likely occurs upon precipitation, which is similar to what we have observed previously in attempts to isolate high-valent Mn-oxo corrolazines in the solid state.

NR Group Transfer. The brown complex **2**, generated from the reaction of chloramine-T and [$Fe^{III}(TBP_8Cz)$], was next examined for its ability to transfer the NTs group to phosphine substrates. The analogous reaction with corrole derivatives (e.g. [Mn^V(tpfc)(NAr)]) and phosphine substrates occurs smoothly, and has yielded kinetic and mechanistic information regarding NR group transfer.[66] Reaction of [$Fe^{IV}(TBP_8Cz^{+\bullet})(NTs)$] (freshly prepared in situ) with excess triphenylphosphine (Scheme 2) led to the isosbestic return of the spectrum for [$Fe^{III}(TBP_8Cz)$] as shown in Figure 3. Production of the two-

dx.doi.org/10.1021/ic400280x | Inorg. Chem. 2013, 52, 4668−4682

Scheme 1. Reaction of $Fe^{III}(TBP_8Cz)$ with Chloramine-T

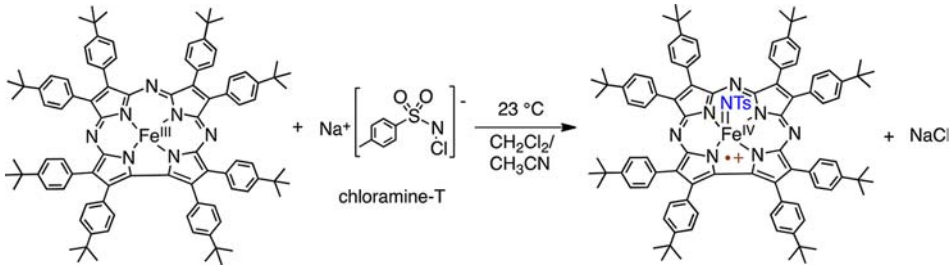

Scheme 2. Reaction of $[Fe^{IV}(TBP_8Cz^{+\bullet})(NTs)]$ with PPh_3

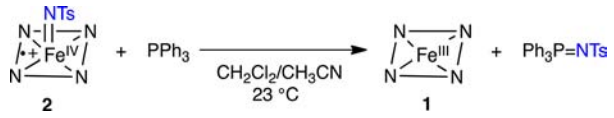

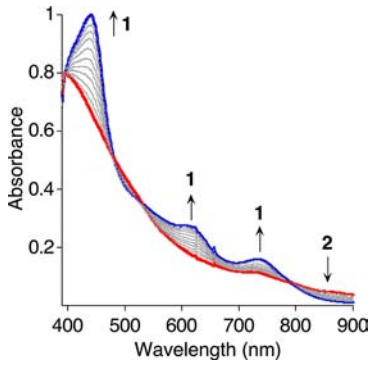

Figure 3. Time-resolved UV−vis spectra of $[Fe^{IV}(TBP_8Cz^{+\bullet})(NTs)]$ + PPh_3 (30 equiv) at 23 °C in CH_2Cl_2/CH_3CN (100:1 v:v).

electron-reduced Fe^{III} product is consistent with the formulation of $[Fe^{IV}(TBP_8Cz^{+\bullet})(NTs)]$, which is two oxidizing equivalents above that of the Fe^{III} starting material. Analysis of the reaction mixture by ^{31}P NMR following addition of PPh_3 reveals a single peak at 14.8 ppm (Figure S11). This peak matches that seen for the expected phosphorane product, $Ph_3P{=}NTs$, providing confirmation of NTs transfer to the phosphine substrate. No signal for unreacted PPh_3 was observed by ^{31}P NMR at the end of the NTs transfer reaction. This observation is consistent with the lack of a ^{31}P signal for independent solutions of $[Fe^{III}(TBP_8Cz)]$ + excess PPh_3, which is likely due to paramagnetic effects from the Fe^{III} complex on PPh_3. The PPh_3 also may coordinate to one or both axial positions at the Fe^{III} center, enhancing the paramagnetic influence.

The generation of $[Fe^{IV}(TBP_8Cz^{+\bullet})(NTs)]$ and subsequent reaction with PPh_3 was monitored by ^1H NMR spectroscopy (Figure S13). The initial spectrum for the Fe^{III} complex **1** reveals paramagnetically shifted peaks between −10 and +15 ppm. Addition of a slight excess of chloramine-T causes the clear disappearance of the paramagnetic signals for **1**, revealing a featureless paramagnetic spectrum for the iron-imido complex **2**. Subsequent addition of excess PPh_3 to the reaction mixture causes an immediate return of the peaks from −10 to 15 ppm associated with the starting complex **1**. These data are nicely consistent with the proposed mechanism of formation of the iron-imido complex and subsequent NTs transfer to PPh_3, which also causes the concomitant return of the Fe^{III} starting material.

Preliminary investigation of the reaction of the imido complex **2** with styrene was also performed to determine its potential reactivity toward aziridination of alkene substrates. As seen in Figure S14, a titration experiment with styrene leads to the reduction of **2** back to the starting Fe^{III} complex **1**, but a very large excess of substrate (48 000 equiv) is needed for this reaction to go to completion over a 25 min period. These data suggest that **2** is a very sluggish NR transfer agent for alkene substrates, and this finding is consistent with the general, inherent stability of **2** in solution at room temperature compared to other high-valent Fe-imido complexes. Given the low reactivity of **2** toward styrene, further studies regarding aziridination of styrene or other substrates were not pursued at this time.

Turnover. The UV−vis and NMR data suggested that the reactions involving the generation of the Fe=NTs complex and the subsequent NR transfer to PPh_3 were relatively fast, and therefore we attempted to determine if catalytic turnover could be achieved. The NR transfer reaction was run under catalytic conditions with a small excess of oxidant (3 equiv) and PPh_3 substrate (10 equiv). The initial formation of **2** from **1** + chloramine-T was first confirmed by UV−vis spectroscopy, and then the substrate was added immediately to initiate the NR transfer reaction. As seen in Figure 4, monitoring of this

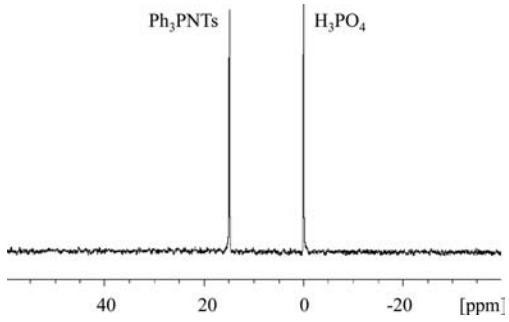

Figure 4. ^{31}P NMR spectrum showing the production of $Ph_3P{=}NTs$ from the reaction of $[Fe^{III}(TBP_8Cz)]$ + chloramine-T trihydrate (3 equiv) + PPh_3 (10 equiv) after 15 min in CD_2Cl_2/CD_3CN at 23 °C.

reaction by ^{31}P NMR showed the rapid production of $Ph_3P{=}NTs$ with no other phosphorane products. The catalytic cycle is summarized in Scheme 3. A background reaction does occur in the absence of **1** under these conditions; however, a significant amount of triphenylphosphine oxide is also produced in this case (Figure S12). The $OPPh_3$ is presumably obtained from oxidation of PPh_3 by hypochlorite anion (OCl^-), which is known to readily form from chloramine-T and exogenous H_2O. There is no $OPPh_3$ observed by ^{31}P NMR in Figure 4, indicating that the catalytic NR transfer must be highly efficient, preventing any background reaction from occurring. We can

dx.doi.org/10.1021/ic400280x | Inorg. Chem. 2013, 52, 4668−4682

Scheme 3. Catalytic Turnover

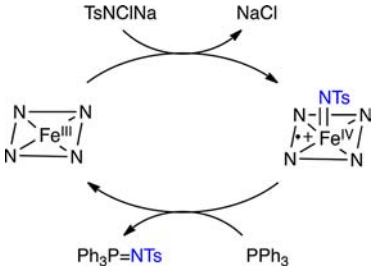

conclude that **1** is capable of catalytic turnover in the NR transfer to phosphines, and that the high-valent iron imido complex **2** is the likely active oxidant in the catalytic cycle.

Kinetics of NR Group Transfer. The kinetics of the reaction between $[Fe^{IV}(TBP_8Cz^{+\bullet})(NTs)]$ and PPh_3 were examined at 23 °C to gain further insight into the reaction mechanism for NR group transfer. The Fe═NTs complex was generated in situ, and excess PPh_3 (30−75 equiv) was added to yield pseudo-first-order conditions. An example of time-resolved UV−vis spectra used for kinetic measurements is shown in Figure 3. Monitoring this transformation at 440 nm over time gives the plot in Figure 5, which was satisfactorily fit

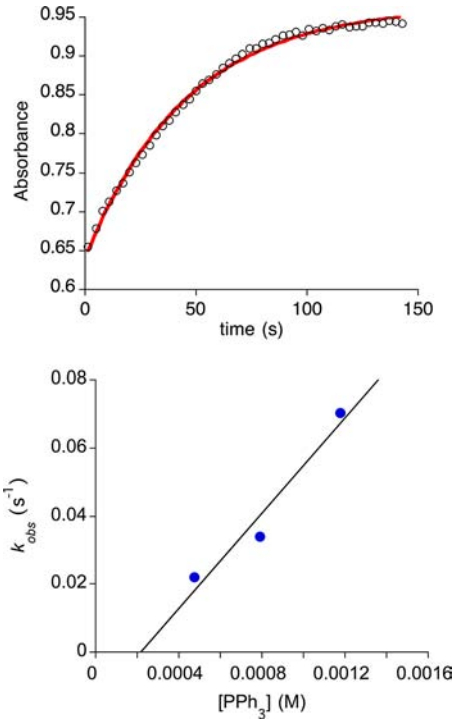

Figure 5. Representative change in absorbance at 440 nm vs time for **2** + PPh_3 corresponding to the return of $Fe^{III}(TBP_8Cz)$ (open circles), and best fit line (red) (top). Plot of the pseudo-first-order rate constants (k_{obs}) vs $[PPh_3]$ (bottom). A second-order rate constant of 70(15) M^{-1} s^{-1} was obtained from the best fit line (black).

with a first-order kinetics model and yielded a k_{obs} = 0.022 s^{-1}. The concentration of PPh_3 was varied and led to a linear correlation of k_{obs} versus $[PPh_3]$ as shown in Figure 5, consistent with an overall second-order rate law of rate = $k_2[Fe^{IV}(TBP_8Cz^{+\bullet})(NTs)][PPh_3]$. The slope of this plot gave a derived second-order rate constant of 70(15) M^{-1} s^{-1}. In comparison, the Mn^V-imido corrole $[Mn^V(tpfc)(NMes)]$ underwent NR group transfer to PPh_3 with a rate constant of 0.71(5) M^{-1} s^{-1}.[66] Thus, the Fe═NTs corrolazine exhibits a 100-fold rate enhancement over an Mn^V imido corrole analogue. These findings are in line with the enhanced reactivity of high-valent iron-oxo versus manganese-oxo corrolazines.[40] In addition, the electron-withdrawing nature of a tosyl group, as compared to a 2,4,6-trichlorophenyl substituent, can be expected to enhance the electrophilicity of **2** and make it more reactive for NR group transfer to nucleophiles such as PPh_3.

Structural Characterization of an NR Group Transfer Product. Efforts were made to obtain single crystals for structural characterization of the phosphine product following reaction of $[Fe^{IV}(TBP_8Cz^{+\bullet})(NTs)]$ with PPh_3. An NMR sample of this reaction mixture in CD_2Cl_2/CD_3CN was allowed to stand for two weeks, affording black crystalline blocks suitable for X-ray diffraction. The structure revealed an iron corrolazine complex with a phospharaniminato ligand coordinated in the axial position, corresponding to $[Fe^{IV}(TBP_8Cz)(NPPh_3)]$ (**3**). A displacement ellipsoid plot for complex **3** is shown in Figure 6, and selected bond distances and angles are

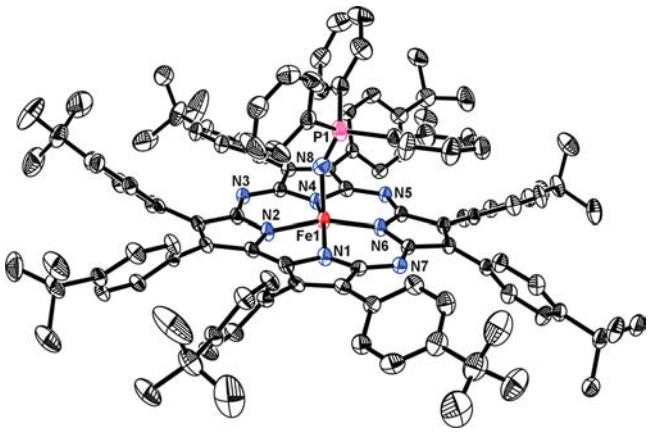

Figure 6. Displacement ellipsoid plot (50% probability level) of $[Fe(TBP_8Cz)(NPPh_3)]$ (**3**). H atoms and disorder are omitted for clarity.

given in Table 1. The tosyl substituent is absent, presumably having been hydrolytically cleaved from the initial Ph_3P═NTs product during crystallization. The remaining anionic Ph_3P═N^- axial ligand indicates that the iron is formally in the +4 oxidation state. We attempted to model the donor atom attached to Fe as an oxygen atom given the possibility of forming $OPPh_3$ in the reaction mixture. However, substitution of O for N in the axial position invariably leads to an unusually large thermal ellipsoid (Figure S3). In addition, substitution of O for N does not alter bond distances significantly, and the resulting P—O bond length would be unusually short (Table 2). These results rule out the presence of an $OPPh_3$ axial donor in **3**. The structural parameters for **3** are also not reasonable for a protonated Ph_3P═NH ligand, and no evidence for a hydrogen atom could be found in the final difference Fourier maps.

To our knowledge there are only two other crystallographically characterized mononuclear Fe—N═PPh_3 complexes reported to date, and relevant structural data for these complexes are given in Table 2. These iron complexes are four-coordinate iron(II) species derived from sterically encumbered tris(carbene)borate ancillary ligands. The Fe−N distance for

dx.doi.org/10.1021/ic400280x | Inorg. Chem. 2013, 52, 4668−4682

Table 1. Selected Bond Distances (Å) and Angles (deg) for 3, 4a, and 4b

	3	4a	4b
Fe(1)−N(1)	1.840(3)	1.843(2)	1.840(2)
Fe(1)−N(2)	1.844(3)	1.849(2)	1.848(2)
Fe(1)−N(4)	1.862(3)	1.867(2)	1.864(2)
Fe(1)−N(6)	1.866(3)	1.866(2)	1.865(2)
Fe(1)−$(N_{pyrrole})_{plane}$	0.292	0.291	0.291
Fe(1)−$(23\text{-atom})_{core}$	0.271	0.262	0.259
C_β−C_β (av)	1.393	1.388	1.390
C_α−C_β (av)	1.446	1.448	1.447
C_α−C_α (C4−C5)	1.425(5)	1.436(4)	1.430(4)
C_α−$N_{pyrrole}$(av)	1.373	1.367	1.369
C_α−N_{meso} (av)	1.338	1.338	1.339
Fe1−X (X = N8 or O1)	1.963(3)	2.002(2)	2.001(2)
P(1)−X	1.427(3)	1.494(2)	1.500(2)
N(1)−Fe(1)−N(2)	80.9(1)	81.12(9)	81.1(1)
N(2)−Fe(1)−N(4)	90.2(1)	90.45(9)	90.3(1)
N(4)−Fe(1)−N(6)	92.9(1)	92.62(9)	92.6(1)
N(6)−Fe(1)−N(1)	90.4(1)	90.17(9)	90.3(1)
N(1)−Fe(1)−X	97.9(1)	98.60(9)	98.50(9)
N(2)−Fe(1)−X	95.9(1)	96.13(8)	95.95(9)
N(4)−Fe(1)−X	100.1(1)	99.30(8)	99.47(9)
N(6)−Fe(1)−X	101.9(1)	101.72(8)	101.85(9)
Fe(1)−X−P(1)	154.5(2)	154.5(1)	154.4(1)

$[Fe^{IV}(TBP_8Cz)(NPPh_3)]$ of 1.963(3) Å is considerably longer than the Fe−N distances seen for the tris(carbene)borate complexes (Fe−N = 1.807(2)−1.894(2) Å). The shorter Fe−N bonds in the latter complexes may be assigned to the $NPPh_3$ ligand functioning as both a σ- and π-donor to the metal. In these approximate C_3-symmetric complexes, the d_{xz}/d_{yz} orbitals can serve as π-acceptors, whereas in the tetragonal Cz complex the orbitals of similar parentage are π^* in character with respect to the Fe−N bond and are partly filled, leading to the elongated Fe−N distance. In contrast, the N−P distance for **3** is significantly shorter than the N−P distances found in the other Fe—N═PPh_3 complexes in Table 2. The origin of this discrepancy is not known at this time, although the N−P distance for **3** is clearly shorter than that expected for either M−$OPPh_3$ or M−(H)$NPPh_3$ complexes, as seen in Table 2.

Efforts to characterize a bulk crystalline sample of $[Fe^{IV}(TBP_8Cz)(NPPh_3)]$ by ESIMS(+) revealed an isotopic cluster centered at m/z 1689.7, whose main peak was +2 above that expected for $[Fe(TBP_8Cz)(NPPh_3)]^{+\bullet}$, but a close match for $[Fe(TBP_8Cz)(OPPh_3)]^{+\bullet}$ (theoretical m/z 1689.8, see Supporting Information). However, the isotope pattern did not fit well for the $OPPh_3$ complex, and suggested that a possible mixture of Fe−$NPPh_3$ and Fe−$OPPh_3$ products crystallized in the same bulk material. This result prompted the analysis of a new batch of crystals from the PPh_3 reaction by X-ray diffraction. A unit cell check on an independently prepared crystal from the PPh_3 reaction mixture revealed a similar cell to that obtained for **3**. However, we speculated that an Fe^{III}−$OPPh_3$ complex might have nearly identical unit cell dimensions to those of **3**, and thus, another full set of data was collected. The structure solution for this second crystal revealed an $OPPh_3$ rather than $NPPh_3$ axial ligand. The crystal structure of this complex, $[Fe^{III}(TBP_8Cz)(OPPh_3)]$ (**4a**), is provided in the Supporting Information, and relevant bond distances and angles are given in Table 1. In this case, the presence of an O atom was confirmed, but the refinement of an N atom in the axial position was attempted. As expected, an N atom in this position led to a significantly smaller thermal ellipsoid, and three residual electron density peaks as large as 0.69 e^- $Å^{-3}$ were found at 0.43−0.48 Å from the N atom, which strongly suggests that not enough electron density has been assigned to this atomic site. The metrical parameters for the second crystal structure from the reaction of $[Fe(TBP_8Cz^{+\bullet})(NTs)]$ + PPh_3 are fully consistent with an Fe^{III}−$OPPh_3$ complex. These findings indicate that a mixture of Fe-$NPPh_3$ and Fe-$OPPh_3$ products ultimately form in the PPh_3 reaction and both crystallize under the same conditions.

Synthesis of $[Fe^{III}(TBP_8Cz)(OPPh_3)]$. The $Fe^{III}(OPPh_3)$ complex was independently prepared for comparison purposes. Addition of excess $OPPh_3$ to a solution of $[Fe^{III}(TBP_8Cz)]$ led to the crystalline complex $[Fe^{III}(TBP_8Cz)(OPPh_3)]$ (**4b**) in good yield (Scheme 4). A displacement ellipsoid plot is shown in Figure 7, and selected bond distances and angles are given in Table 1. The metrical parameters match well with those found for **4a**. The UV−vis and ESIMS spectra for **4b** are shown in Figure 8. The mass spectral data show a dominant cluster centered at m/z 1689.7, and its position and isotope pattern match nicely for $[Fe(TBP_8Cz)(OPPh_3)]^+$. This result can be contrasted with Figure S4, in which a different isotope pattern was obtained for the mixture of **3** + **4a** from the chloramine-T reaction. The UV−vis spectrum is similar to that of the Fe^{III} starting material, but a blue-shift of ∼15 nm is seen for the 732 nm band, resulting from coordination of $OPPh_3$ to Fe^{III}. Elemental analysis confirmed the high purity of **4b** as a bulk crystalline solid, and this material provided a key benchmark for further studies, including ^{31}P NMR and Mössbauer spectroscopies, while also confirming our assignment of the **3** + **4a** mixture from the PPh_3 oxidation reaction.

Scheme 4. Synthesis of $Fe^{III}(TBP_8Cz)(OPPh_3)$

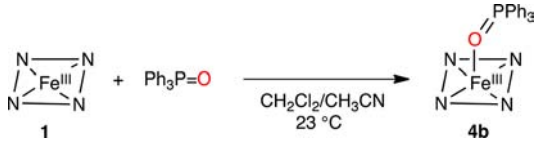

Monitoring Production of Hydrolyzed Products by ^{31}P NMR Spectroscopy. The reaction of $[Fe^{IV}(TBP_8Cz^{+\bullet})$-

Table 2. Comparison of Selected Bond Distances (Å) for Metal-$XPPh_3$ Compounds (X = N, O)

	M−X	P−X	ref
$[Fe^{IV}(TBP_8Cz)(NPPh_3)]$ (**3**)	1.963(3)	1.427(3)	this study
$[Fe^{III}(TBP_8Cz)(OPPh_3)]$ (**4b**)	2.001(2)	1.500(2)	this study
M-(H)$NPPh_3$ (M = Os, Cu, Zr, Ta)	1.931−2.367	1.511−1.843	67, 81−84
Fe^{III}−$OPPh_3$	1.912−2.056	1.483−1.507	85−89
$PhB(^tBuIm)_3Fe^{II}$−$NPPh_3$	1.894(2)	1.527(2)	59
$PhB(MesIm)_3Fe^{II}$−$NPPh_3$	1.807(2)−1.855(2)	1.524(2)−1.549(2)	90

dx.doi.org/10.1021/ic400280x | Inorg. Chem. 2013, 52, 4668−4682

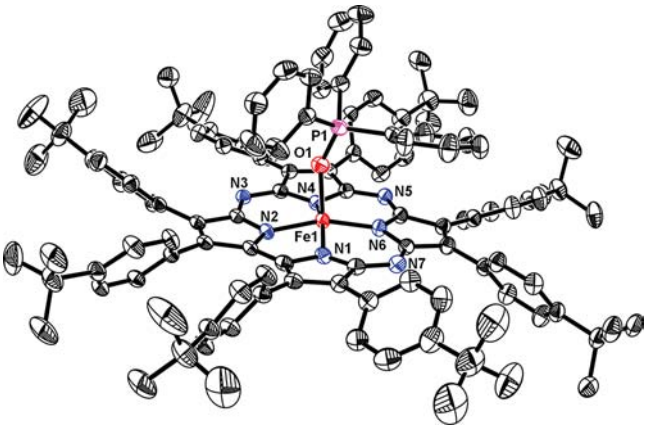

Figure 7. Displacement ellipsoid plot (50% probability level) of $[Fe^{III}(TBP_8Cz)(OPPh_3)]$ (**4b**). H atoms and disorder are omitted for clarity.

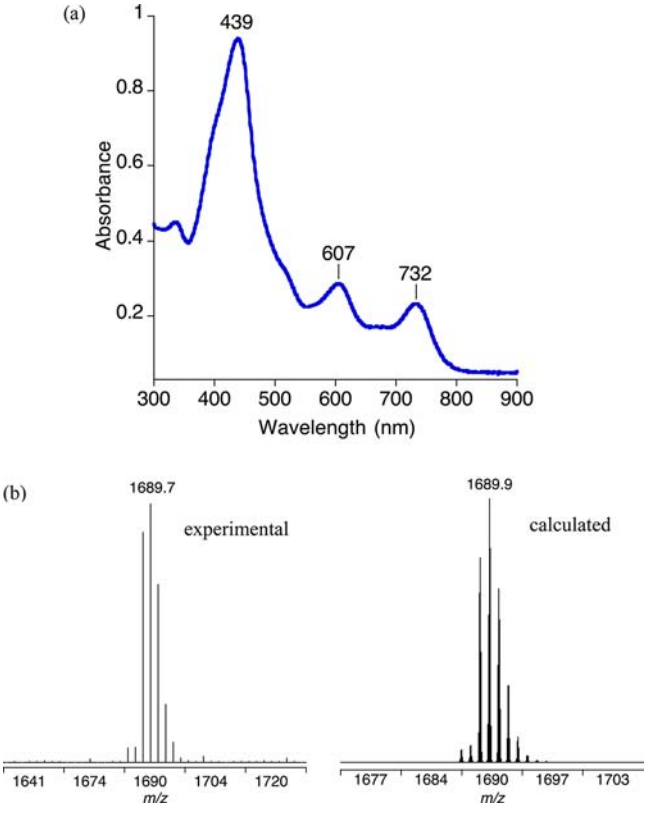

Figure 8. (a) UV–vis and (b) ESIMS spectra for $[Fe^{III}(TBP_8Cz)(OPPh_3)]$ (**4b**) as a crystalline solid dissolved in CH_2Cl_2.

(NTs)] (**2**) + PPh_3 was monitored by ^{31}P NMR spectroscopy over an extended time-course to gain insight into the mechanism of NR transfer and formation of the final phosphine-derived products $[Fe^{IV}(TBP_8Cz)(NPPh_3)]$ (**3**) and $[Fe^{III}(TBP_8Cz)(OPPh_3)]$ (**4**). Examination of the reaction mixture after day 1 shows only the Ph_3PNTs product, as expected (Figure 9). Following this initial spectrum, there is a slow build-up of the detosylated Ph_3PNH compound at 21.8 ppm (verified by comparison with an authentic sample). By day 7, a broad peak appears at 27.9 ppm, which then grows in intensity after a further week of reaction (day 14). An independent sample of pure $[Fe^{III}(TBP_8Cz)(OPPh_3)]$ (**4b**) exhibited the same broad peak in the ^{31}P NMR spectrum

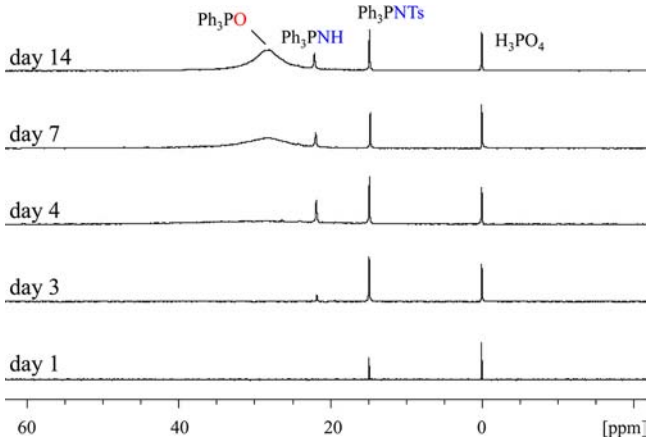

Figure 9. ^{31}P NMR spectra of the reaction of $[Fe^{III}(TBP_8Cz)]$ + chloramine-T trihydrate (3 equiv) + PPh_3 (10 equiv) in CD_2Cl_2/CD_3CN over 2 weeks.

(Figure S7). Thus, the ^{31}P NMR time-course shows the production of all three phosphorus products, Ph_3PNTs, $Ph_3PN(H)$, and Ph_3PO, over a two-week period.

Mechanism. A proposed mechanism for NR group transfer and generation of the different phosphine products is shown in Scheme 5. Initial formation of the Fe═NTs complex is followed by nucleophilic attack of PPh_3 to give Ph_3PNTs and an iron(III) corrolazine. The Ph_3PNTs may be activated by Fe^{III} toward hydrolytic cleavage of the tosyl group, resulting in production of Ph_3PNH. Coordination of this phosphinimine product can then lead to the formation of $Fe^{IV}(NPPh_3)$, following oxidation of an Fe^{III} precursor. Although the identity of the oxidant is not known, oxidation of Fe^{III} to Fe^{IV} is likely facilitated by a strong axial donor such as Ph_3PN^-. The generation of Ph_3PO occurs upon hydrolysis of Ph_3PNH, which is known to readily hydrolyze to Ph_3PO and NH_4OH in the presence of residual water.[67] The presence of Ph_3PO can then give rise to the final $Fe^{III}(OPPh_3)$ complex. This mechanism accounts for both the NMR time-course experiments and the observation of the different products from X-ray crystallography.

EPR and Mössbauer Spectroscopies. To obtain information about the oxidation states and spin states of the Fe corrolazine complexes described here, EPR and Mössbauer spectra were collected. Previous work on iron corrole complexes[68−71] has shown that it is often difficult to determine their electron configurations due to the noninnocent nature of the corrolate ligand. Similar complications arise with the related iron corrolazines presented in this study. Further complexity is to be expected when Mössbauer spectra of frozen solutions are collected because corrolazines, like other porphyrinoid compounds, are prone to aggregation, which can lead to intermolecular spin–spin relaxation.[72−74] For these reasons the Mössbauer and EPR data have to be treated as a whole. To support the Mössbauer and EPR assignments we ran a set of DFT calculations in tandem with the experiments.

A solid state, crystalline sample of **4b** formed from the reaction of $[Fe^{III}(TBP_8Cz)]$ with Ph_3PO provides a well-defined reference compound for spectroscopic measurements because the structure has been determined with high precision by single-crystal X-ray diffraction, and the oxidation state of the iron center can be definitively assigned as +3. A sample of **4** exhibits a Mössbauer spectrum at 5.3 K with a single, sharp

dx.doi.org/10.1021/ic400280x | Inorg. Chem. 2013, 52, 4668−4682

Scheme 5. Proposed Mechanism

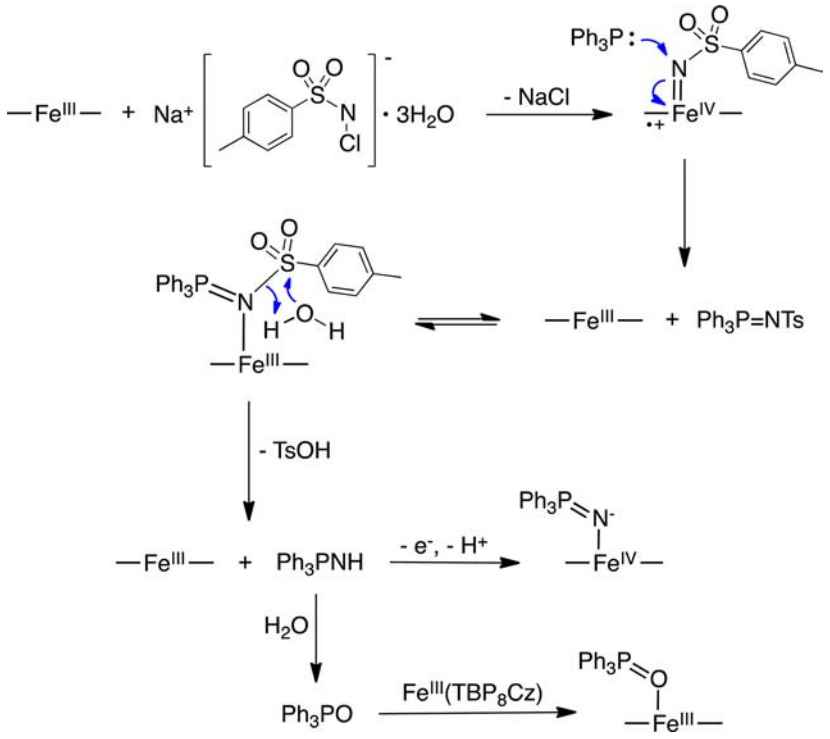

quadrupole doublet (δ = 0.13 mm s^{-1}; ΔE_Q = 4.40 mm s^{-1}, Figure 10). The isomer shift is consistent with an intermediate spin (S = $^3/_2$) Fe^{III} ion as seen by comparison with other intermediate spin iron(III) complexes (see Table 5 in ref 56), and the large quadrupole splitting is in part due to the square pyramidal geometry (see bond angles above). Indeed, the square pyramidal geometry of the iron center revealed by the crystal structure of [Fe^{III}(TBP$_8$Cz)(OPPh$_3$)] (Figure 7) and the presence of the strong-field equatorial corrolazine ligand should greatly destabilize the $d_{x^2-y^2}$ orbital relative to the other d orbitals and therefore stabilize the S = $^3/_2$ state relative to the high spin S = $^5/_2$ state. The intermediate spin state of this compound is further confirmed by EPR spectroscopy. The X-band EPR spectrum of a crystalline sample of **4** dissolved in toluene and measured at 15 K (Figure 11) shows an axial signal with $g_\perp$ = 4.43, $g_\parallel$ = 1.99, which is typical for an S = $^3/_2$ ion.

In comparison, the Mössbauer spectrum of solid [Fe^{III}(TBP$_8$Cz)], which lacks an OPPh$_3$ axial ligand, was measured at 293 K and consists of two quadrupole doublets (δ = 0.06 mm s^{-1}, ΔE_Q = 4.00 mm s^{-1} and δ = 0.30 mm s^{-1}, ΔE_Q = 1.00 mm s^{-1}, Figure 10) in a ratio of approximately 3:1.

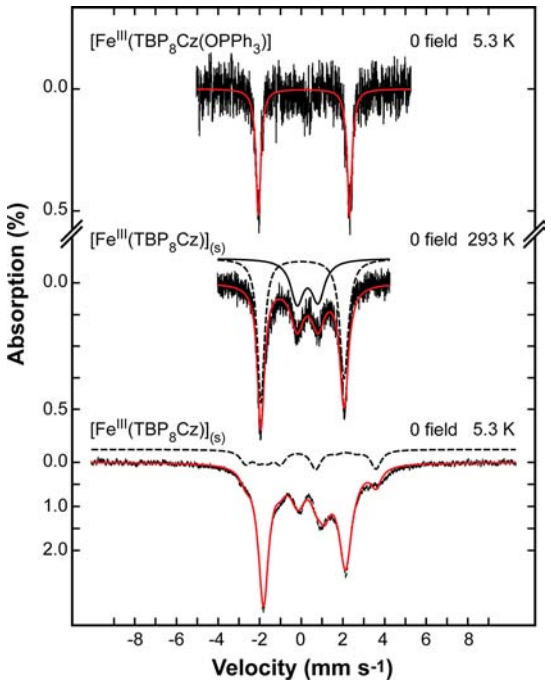

Figure 10. Mössbauer spectra of a crystalline sample of [Fe^{III}(TBP$_8$Cz)(O═PPh$_3$)] (**4b**) measured at 5.3 K and a solid sample of [Fe^{III}(TBP$_8$Cz)] (**1**) measured at 293 K (solid black line = high spin Fe^{III}; dashed black line = intermediate spin Fe^{III}) and 5.3 K with no applied magnetic field (dashed line = slow relaxing intermediate spin Fe^{III}). The red lines show the best fit to the data.

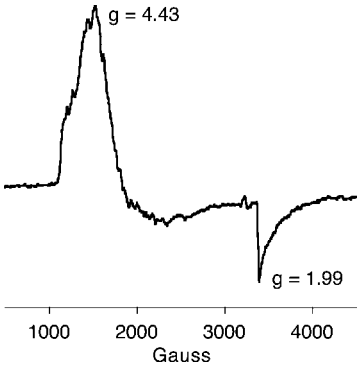

Figure 11. X-band EPR spectrum at 15 K of crystalline [Fe^{III}(TBP$_8$Cz)(OPPh$_3$)] (**4b**) dissolved in toluene. Experimental conditions: frequency = 9.49 GHz, microwave power = 0.201 mW, modulation amplitude 10.0 G, modulation frequency = 100 kHz.

dx.doi.org/10.1021/ic400280x | Inorg. Chem. 2013, 52, 4668−4682

These parameters and intensities are similar to those recently reported for [$Fe^{III}(TBP_8Cz)$] by Nakamura and co-workers,[75] who measured temperature-dependent Mössbauer spectra down to 77 K. In this study the quadrupole splitting was seen to be temperature-independent, but the isomer shift increased with a decrease in temperature, as one would expect, as a result of the second-order Doppler shift.[76] As seen in Figure 10, the spectrum at 5.3 K for **1** consists of two quadrupole doublets with a slight increase in the isomer shifts (δ = 0.15 mm s^{-1} and δ = 0.47 mm s^{-1}) as compared to the data at 293 K. These isomer shifts can be assigned to a mixture of intermediate spin Fe^{III} and high spin Fe^{III} ($S = {}^5/_2$) ions. Additionally, there is a broad component (~20%, dashed line Figure 10) caused by slow relaxation of the intermediate spin iron(III) centers relative to the Mössbauer time scale of ~10^7 s^{-1}, resulting in splitting of the nuclear magnetic spin states and giving rise to the broad spectrum observed. The parameters used to simulate this magnetic spectrum were those used to fit the frozen solution spectrum of [$Fe^{III}(TBP_8Cz)$] described below.

Dissolution of the [$Fe^{III}(TBP_8Cz)$] complex in toluene provides Mössbauer spectra that help to clarify the spectral assignments. A frozen toluene solution of the Fe^{III} complex produces a single quadrupole doublet at 100 K (δ = 0.11 mm s^{-1}, ΔE_Q = 3.96 mm s^{-1}, Figure 12), consistent with the

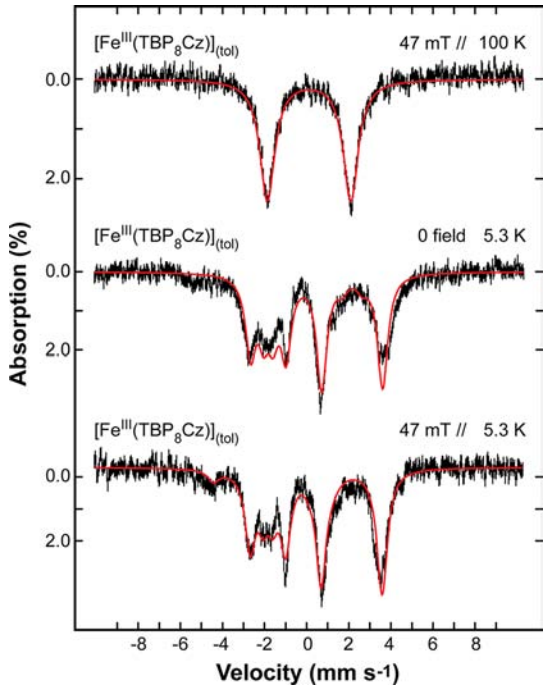

Figure 12. Mössbauer spectra of [$Fe^{III}(TBP_8Cz)$] dissolved in toluene and measured at 100 K with an applied magnetic field of 47 mT parallel to the γ-rays, 5.3 K with no magnetic field and 5.3 K with an applied magnetic field of 47 mT parallel to the γ-rays. The red line through the data shows the best fit using the parameters given in the text.

presence of a pure intermediate spin species. If the sample is then suitably diluted and carefully frozen,[72] the spectra collected at the lower temperature of 5.3 K are clearly in the slow relaxation regime (Figure 12), and can be fitted to a single $S = {}^3/_2$ species. This result is in good agreement with EPR spectra of the same complex in a frozen solution of toluene, which revealed an intermediate spin iron(III) spectrum at 15 K.[42] Careful comparison of the Mössbauer spectra in the presence and absence of a small magnetic field (47 mT) allows this species to be fitted with the values δ = 0.15 mm s^{-1}; ΔE_Q = +3.98 mm s^{-1}; $D = -4$ cm^{-1}; $E/D = 0$; $A_x = A_y = 19$ T, $A_z = 6$ T, which are comparable with intermediate spin Fe^{III} tetraamido complexes.[77] We can conclude that dissolution in toluene provides a uniform environment for complex **1** and leads to the observation of a single iron(III) intermediate spin ground state, in contrast to the solid state, in which stacking or other aggregation effects appear to give rise to a mixture of the two different spin states $S = {}^3/_2$ and $S = {}^5/_2$ for **1**.

The third possible spin state for an Fe^{III} species is a low-spin ($S = {}^1/_2$) configuration, and this state can be accessed for iron(III) corrolazine by addition of excess pyridine. Previous work has shown that addition of pyridine to [$Fe^{III}(TBP_8Cz)$] gives the axially ligated complex [$Fe^{III}(TBP_8Cz)(py)_2$], which reveals an intense rhombic EPR spectrum (g 2.39, 2.20, 1.90) that is characteristic of a low spin Fe^{III} porphyrinoid compound.[42] The Mössbauer spectrum of this species at 100 K consists of a symmetrical quadrupole doublet (δ = 0.01 mm s^{-1}, ΔE_Q = 3.99 mm s^{-1}, Figure 13). The isomer shift is consistent with low spin Fe^{III}, and indeed the value is lower than that of the intermediate spin species discussed above. At 5.3 K, the spectrum consists of both slow (dashed line, Figure 13) and fast relaxing low spin Fe^{III} signals (δ = 0.03 mm s^{-1}, ΔE_Q = 4.03 mm s^{-1}), as seen for the intermediate spin complex (Figure 10). These parameters are similar to, but slightly larger than, those recently described[75] for the analogous bis(cyano) complex [$Fe^{III}(TBP_8Cz)(CN)_2]^{2-}$ ($\delta = -0.09$ mm s^{-1}, ΔE_Q = 2.74 mm s^{-1} at 77 K).

The Mössbauer spectrum of bulk, crystalline **3** consists of a quadrupole doublet at 293 K (δ = 0.13 mm s^{-1}, ΔE_Q = 4.25 mm s^{-1}, Figure 13). However, a bulk sample of this material consists of both [$Fe^{IV}(TBP_8Cz)(NPPh_3)$] and [$Fe^{III}(TBP_8Cz)$-$(OPPh_3)$] as shown by independent X-ray analysis. An EPR spectrum of a bulk sample of **3** at 15 K revealed only a weak signal with broad features at g 5.39, 2.02 (Figure S10), consistent with the presence of [$Fe^{III}(TBP_8Cz)(OPPh_3)$] as a minor impurity. The Mössbauer spectrum of **3** at 5.3 K can be fitted to an Fe^{IV} (S = 1) species (δ = 0.13 mm s^{-1}; ΔE_Q = 4.25 mm s^{-1}; $D = +5$ cm^{-1}; $E/D = 0$; $A_x = A_y = 8$ T, $A_z = 10$ T; Figure 13) together with [$Fe^{III}(TBP_8Cz)(OPPh_3)$] as a minor component (~10%, fitted with the parameters found for the pure $Fe^{III}(OPPh_3)$ complex). Thus, Mössbauer and EPR spectroscopy are in agreement with the assignment of the bulk crystalline material for **3**. Interestingly, the isomer shift for the Fe^{IV} complex (δ = 0.13 mm s^{-1}) is comparable to the isomer shift found for the intermediate spin Fe^{III} corrolazines, which suggests that the Fe^{IV}–$NPPh_3$ complex may be better described as an intermediate spin Fe^{III} center coupled to a corrolazine π-cation radical. This dichotomy for iron(IV) corroles has been discussed at length by Walker and co-workers,[70] but these two options cannot be distinguished for the current complex from the available data. We note that the quadrupole splitting parameters are distinct for the Fe^{IV} complex **3** (4.25 mm s^{-1}) and the intermediate spin-Fe^{III} complex **4** (4.40 mm s^{-1}), although not by as much as might be expected. Future experimental/computational work may shed light on this issue.

Finally, Mössbauer spectroscopy was also employed to analyze a ^{57}Fe-labeled sample of [$Fe^{IV}(TBP_8Cz^{+\bullet})(NTs)$], which was isolated as a precipitated solid from the reaction

dx.doi.org/10.1021/ic400280x | Inorg. Chem. 2013, 52, 4668–4682

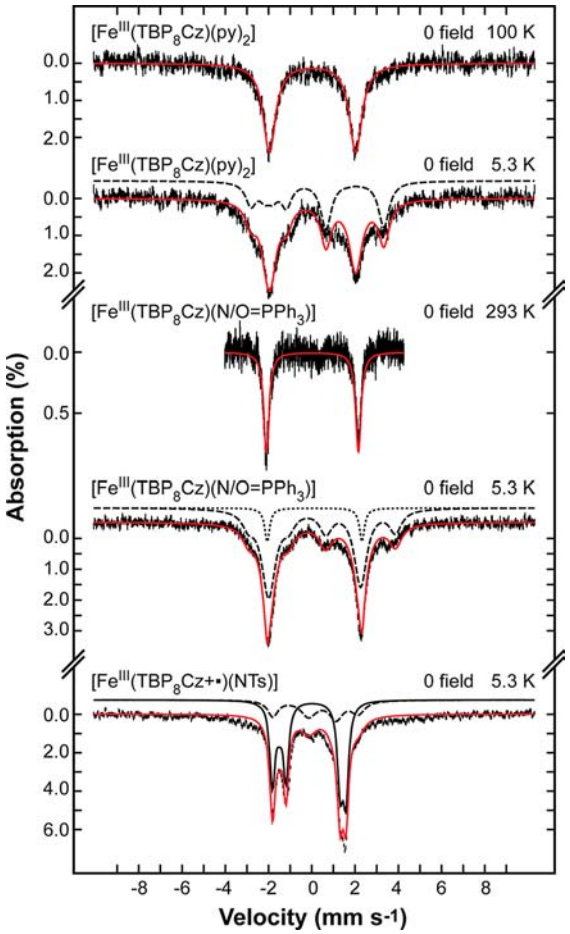

Figure 13. Mössbauer spectra of $[Fe^{III}(TBP_8Cz)]$ dissolved in pyridine at 100 and 5.3 K with no applied field (dashed line = slow relaxing low spin Fe^{III}). Mössbauer spectra of a solid sample of $[Fe^{III}(TBP_8Cz)(N/OPPh_3)]$ measured at 293 and 5.3 K (dotted line = $[Fe^{III}(TBP_8Cz)(OPPh_3)]$; dashed line = $[Fe^{IV}(TBP_8Cz)(NPPh_3)]$). Frozen solution spectrum of $[Fe^{IV}(TBP_8Cz^{+\bullet})(NTs)]$ measured at 5.3 K (dashed line = ~25% $[Fe^{III}(TBP_8Cz)]$). The red line through the data shows the best fit using the parameters given in the text.

mixture of $[Fe^{III}(TBP_8Cz)]$ and chloramine-T. The spectrum measured at 5.3 K in toluene (Figure 13) can be fitted to two species: ~25% of unreacted $[Fe^{III}(TBP_8Cz)]$ (dashed line, parameters given above), and an Fe^{IV} (S = 1) ion antiferromagnetically coupled to a Cz-π-cation-radical (δ = −0.05 mm s^{-1}; ΔE_Q = 2.94 mm s^{-1}; $A_x = A_y$ = 26 T, A_z = 3.5 T; J ~ 30 cm^{-1}). The sign of the quadrupole splitting cannot be unambiguously defined, but if positive, a rotation of the electric field gradient (EFG) relative to the principle axes is required. In fact there is no reason why the principal axes should be collinear and the EFG tensor can be rotated by a set of Euler angles α, β, and γ (0, 105, 0). The low isomer shift and smaller quadrupole splitting of this species as compared to those found for the Fe^{III} complexes strongly suggest that this complex contains an iron(IV) center as proposed.[68] In addition, EPR spectroscopy of this complex at 15 K gives a sharp axial signal with $g_\perp$ = 2.10, $g_\parallel$ = 2.00, consistent with an overall $S = {}^1/_2$ ground state as expected for an Fe^{IV}−Cz-π-cation-radical and in good agreement with the Mössbauer analysis.

Altogether, the Mössbauer data show consistent findings across all species as summarized in Table 3. The intermediate spin $S = {}^3/_2$ Fe^{III} species all have isomer shifts of ~+0.13 mm s^{-1}. The isomer shift for $[Fe^{IV}(TBP_8Cz)(NPPh_3)]$ also falls in this range, and this complex may be best described as an Fe^{III} coupled to a π-radical-cation. Conversion to a low spin Fe^{III} center by addition of pyridine to form $[Fe^{III}(TBP_8Cz)(py)_2]$ lowers the isomer shift to +0.03 mm s^{-1}. Further oxidation to form $[Fe^{IV}(TBP_8Cz^{+\bullet})(NTs)]$ leads to an isomer shift of −0.05 mm s^{-1}, consistent with a high-valent iron(IV) ion.

Computational Studies. To further confirm the spectroscopic data and gain structural insight into the iron-imido complex we have calculated the Mössbauer and EPR parameters of $[Fe^{IV}(H_8Cz^{+\bullet})(NTs)]$ in both the doublet and quartet spin states using DFT. To reduce calculation time a model where the eight peripheral ^{t}Bu-phenyl groups from the corrolazine ring were replaced by hydrogen atoms was implemented, H_8Cz. Initial geometric optimization led to a structure with reasonable bond lengths (Figure 15). The Fe−N

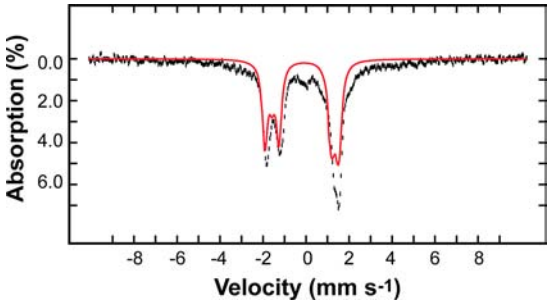

Figure 14. Mössbauer spectra of $[Fe^{IV}(TBP_8Cz^{+\bullet})(NTs)]$ measured at 5.3 K. Overlaid is a simulation (red line) using the parameters determined by DFT with the EFG and A rotated by the following Euler angles (19, 100, 51) and (70, 92, 3).

Table 3. Mössbauer Parameters for Iron Corrolazine Complexes

		spin state	δ (mm s^{-1})	ΔE_Q (mm s^{-1})	Γ (mm s^{-1})	D (cm^{-1})	E/D	$A_x/g_n\mu_n$ [a] (T)	$A_y/g_n\mu_n$ [a] (T)	$A_z/g_n\mu_n$ [a] (T)
$[Fe^{III}(TBP_8Cz)]$		$^3/_2$	0.15	+3.98	0.6	−4	0	19	19	6
$[Fe^{III}(TBP_8Cz)(py)_2]$		$^1/_2$	0.03	4.03	0.7					
$[Fe^{III}(TBP_8Cz)(OPPh_3)]$		$^3/_2$	0.13	4.40	0.3					
$[Fe^{IV}(TBP_8Cz)(NPPh_3)]$		1[b]	0.13	4.25	0.7	+5	0	8	8	10
$[Fe^{IV}(TBP_8Cz^{\bullet+})(NTs)]$	expt	$^1/_2$[c]	−0.05	2.95	0.3			26	26	3.5
	calcd	$^1/_2$[d]	−0.12	+2.92				−4.8	24.0	30.9

[a]The sign of the hyperfine coupling constants cannot be determined. [b]The spin state is not fully determined and can be considered an intermediate spin Fe^{III} coupled to a radical cation, as the isomer shift suggests. [c]The S = 1 Fe^{IV} is antiferromagnetically coupled to a $S = {}^1/_2$ radical cation with an exchange coupling constant of ~30 cm^{-1}. The electric field gradient (EFG) is rotated using the following Euler angles (0, 105, 0). [d]η = 0.38. To fit experiment, both the EFG and A tensors have to be rotated by the following Euler angles (19, 100, 51) and (70, 92, 3), respectively, because the principal axes used are different.

dx.doi.org/10.1021/ic400280x | Inorg. Chem. 2013, 52, 4668−4682

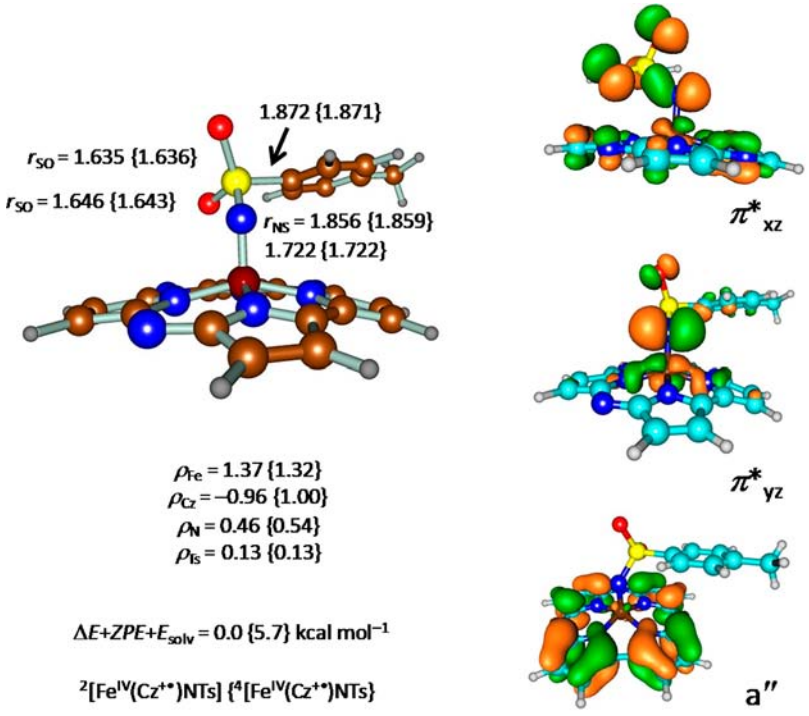

Figure 15. DFT calculated structures of ^{2,4}[Fe^{IV}(H_8Cz$^{+\bullet}$)(NTs)] with bond lengths in angstroms and group spin densities (ρ) in atomic units. Also given are the spin state energy differences in kcal mol^{-1} as calculated at UB3LYP/B2//UB3LYP/B1 including solvent and zero-point corrections. Orbital drawings of the singly occupied molecular orbitals are given on the right.

bond length of 1.722 Å is comparable to other iron-imido complexes both experimental and calculated.[8,78] The doublet spin state is the ground state and is found to lie 5.7 kcal mol^{-1} below the quartet spin state, consistent with the spectroscopic results given above. The spin densities were then calculated and molecular orbitals analyzed, which revealed two unpaired electrons in the $\pi^*_{xz/yz}$ orbitals antiferromagnetically coupled to a single electron in the a″-type Cz orbital. The orbital shapes and the electronic configuration show resemblance to that calculated for [Mn^{V}(H_8Cz$^{+\bullet}$)(O)], which also gave single occupation of the a″ orbital.[38] Due to mixing of the atomic $3d_{xz}/3d_{yz}$ orbitals on Fe with $2p_x/2p_y$ orbitals on nitrogen, the π^*_{xz} and π^*_{yz} orbitals are mixed iron/nitrogen antibonding orbitals, and consequently, considerable spin density is observed on the nitrogen and tosylate group. This mixing is similar to that observed on the oxo group in heme and nonheme iron(IV)-oxo species.[79,80]

Finally, the Mössbauer and EPR parameters were then calculated and are given in Table 3. The parameters compare favorably with the experimentally determined ones and provide further strong evidence that our understanding of the electronic state is correct. The calculated g values (2.00, 2.03, 2.07) are rhombic rather than axial, but the Mössbauer isomer shift and quadrupole splitting reproduce the experimental data within the error of the calculations. A simulation of the Mössbauer spectrum with these parameters is given in Figure 14 and shows graphically how close the match is. To obtain a reasonable fit both the electric field gradient (EFG) and hyperfine (A) tensors had to be rotated relative to each other. The following Euler angles were used: (19, 100, 51) for the EFG and (70, 92, 3) for A.

CONCLUSIONS

The reaction of [Fe^{III}(TBP_8Cz)] with the NR transfer agent chloramine-T results in the formation of the high-valent iron(IV) terminal imido complex [Fe^{IV}(TBP_8Cz$^{+\bullet}$)(NTs)] (**2**). Previously iron terminal imido complexes have been stabilized through a combination of steric encumbrance and the enforcement of relatively low-coordinate geometries about the iron center. The stability of **2** is likely a consequence of the oxidatively resistant, trianionic corrolazine supporting ligand favoring high-valent iron(IV) together with the strong σ and π donation of the terminal tosylimido donor. The stability of **2** is significant because high-valent, multiply bonded terminal imido complexes of the mid- to late-transition metals are normally considered to be highly reactive, but the data presented here indicates that **2** is much more stable (and consequently less reactive) than is expected for an iron-imido complex. Thus, catalytic mechanisms that rely on proposed intermediates of this type, especially in porphyrinoid chemistry, may need to be carefully scrutinized when identifying the actual oxidizing species.

Mössbauer and EPR spectroscopies show that [Fe^{IV}(TBP_8Cz$^{+\bullet}$)(NTs)] contains a high-valent Fe^{IV} ion with an extra oxidizing equivalent stored on the Cz ring as a π-cation-radical, analogous to the previously described compound-I-like terminal oxo complex [Fe^{IV}(TBP_8Cz$^{+\bullet}$)(O)].[39] This view has been further corroborated by DFT calculations. The spin state of both the imido and oxo complexes is proposed to be a doublet with iron(IV) antiferromagnetically coupled to the Cz π-cation-radical. It was demonstrated that **2** is capable of NR group transfer to triphenylphosphine to give Ph_3PNTs, leading to the two-electron reduction of **2** to give the Fe^{III} complex **1**. Catalytic NR transfer to PPh_3 by **1** was also successful, suggesting that further design of suitable metallocorrolazines (or corroles) may yield potent NR transfer

dx.doi.org/10.1021/ic400280x | Inorg. Chem. 2013, 52, 4668−4682

catalysts. The kinetic data For NR transfer from **2** to PPh_3 was in agreement with the proposed bimolecular mechanism, and a comparison of rate constants shows that **2** exhibits a dramatic rate enhancement (~100-fold) for NR transfer as compared to $Mn^V(NAr)$ corrole analogues. Structural analyses of complexes formed following initial NR transfer reveal that both $[Fe^{IV}(TBP_8Cz)(NPPh_3)]$ and $[Fe^{III}(TBP_8Cz)(OPPh_3)]$ crystallize from the same reaction mixture. A mechanism was described that can account for the NR transfer reactivity of **2** as well as the subsequent formation of the former complexes.

■ ASSOCIATED CONTENT

Ⓢ Supporting Information

Spectroscopic and crystallographic data (CIF), and details of the DFT calculations, including relative and absolute energies, group spin densities, charges, and Cartesian coordinates of all structures. This material is available free of charge via the Internet at http://pubs.acs.org.

■ AUTHOR INFORMATION

Corresponding Author

*E-mail: dpg@jhu.edu (D.P.G.); gjameson@chemistry.otago.ac.nz (G.N.L.J.); sam.devisser@manchester.ac.uk (S.P.d.V.).

Notes

The authors declare no competing financial interest.

■ ACKNOWLEDGMENTS

This work was supported by the NSF (CHE0909587 and CHE1213836 to D.P.G.). P.L. is grateful for the Queen Sirikit Scholarship (Thailand). We thank Dr. Yosra M. Badiei for the synthesis of $^{57}FeCl_2$ and Dr. Victoria J. A. Jameson for help with Mössbauer sample preparation. The computational work was supported by CPU time provided by the National Service of Computational Chemistry Software (NSCCS). D.K. holds a Ramanujan Fellowship from the Department of Science and Technology (DST), New Delhi (India), and acknowledges its financial support (Research Grants SR/S2/RJN-11/2008 and SR/S1/PC-58/2009).

■ REFERENCES

(1) Ertl, G. *Angew. Chem., Int. Ed.* **1990**, *29*, 1219−1227.
(2) Smil, V. *Enriching the Earth: Fritz Haber, Carl Bosch, and the Transformation of World Food Production*; MIT Press: Cambridge, 2004.
(3) Hoffman, B. M.; Dean, D. R.; Seefeldt, L. C. *Acc. Chem. Res.* **2009**, *42*, 609−619.
(4) Seefeldt, L. C.; Hoffman, B. M.; Dean, D. R. *Annu. Rev. Biochem.* **2009**, *78*, 701−722.
(5) Pickett, C. J. *J. Biol. Inorg. Chem.* **1996**, *1*, 601−606.
(6) Svastits, E. W.; Dawson, J. H.; Breslow, R.; Gellman, S. H. *J. Am. Chem. Soc.* **1985**, *107*, 6427−6428.
(7) King, E. R.; Betley, T. A. *Inorg. Chem.* **2009**, *48*, 2361−2363.
(8) King, E. R.; Hennessy, E. T.; Betley, T. A. *J. Am. Chem. Soc.* **2011**, *133*, 4917−4923.
(9) Berry, J. F. *Comments Inorg. Chem.* **2009**, *30*, 28−66.
(10) Mehn, M. P.; Peters, J. C. *J. Inorg. Biochem.* **2006**, *100*, 634−643.
(11) Saouma, C. T.; Peters, J. C. *Coord. Chem. Rev.* **2011**, *255*, 920−937.
(12) Zalatan, D. N.; Du Bois, J. *Top. Curr. Chem.* **2010**, *292*, 347−378.
(13) Müller, P.; Fruit, C. *Chem. Rev.* **2003**, *103*, 2905−2919.
(14) Chow, T. W. S.; Chen, G. Q.; Liu, Y. G.; Zhou, C. Y.; Che, C. M. *Pure Appl. Chem.* **2012**, *84*, 1685−1704.
(15) Eikey, R. A.; Abu-Omar, M. M. *Coord. Chem. Rev.* **2003**, *243*, 83−124.
(16) Abu-Omar, M. M. *Dalton Trans.* **2011**, *40*, 3435−3444.
(17) Smith, J. M.; Subedi, D. *Dalton Trans.* **2012**, *41*, 1423−1429.
(18) To our knowledge, there are only two reported Fe compounds with +6 oxidation state: Berry, J. F.; Bill, E.; Bothe, E.; DeBeer George, S.; Mienert, B.; Neese, F.; Wieghardt, K. *Science* **2006**, *312*, 1937−1941.
(19) Hohenberger, J.; Ray, K.; Meyer, K. *Nat. Commun.* **2012**, *3*, 720.
(20) Mahy, J. P.; Battioni, P.; Mansuy, D.; Fisher, J.; Weiss, R.; Mispelter, J.; Morgensternbadarau, I.; Gans, P. *J. Am. Chem. Soc.* **1984**, *106*, 1699−1706.
(21) Klinker, E. J.; Jackson, T. A.; Jensen, M. P.; Stubna, A.; Juhasz, G.; Bominaar, E. L.; Münck, E.; Que, L., Jr. *Angew. Chem., Int. Ed.* **2006**, *45*, 7394−7397.
(22) Brown, S. D.; Betley, T. A.; Peters, J. C. *J. Am. Chem. Soc.* **2003**, *125*, 322−323.
(23) Moret, M. E.; Peters, J. C. *Angew. Chem., Int. Ed.* **2011**, *50*, 2063−2067.
(24) Betley, T. A.; Peters, J. C. *J. Am. Chem. Soc.* **2003**, *125*, 10782−10783.
(25) Brown, S. D.; Peters, J. C. *J. Am. Chem. Soc.* **2005**, *127*, 1913−1923.
(26) Thomas, C. M.; Mankad, N. P.; Peters, J. C. *J. Am. Chem. Soc.* **2006**, *128*, 4956−4957.
(27) Nieto, I.; Ding, F.; Bontchev, R. P.; Wang, H. B.; Smith, J. M. *J. Am. Chem. Soc.* **2008**, *130*, 2716−2717.
(28) Bowman, A. C.; Milsmann, C.; Bill, E.; Turner, Z. R.; Lobkovsky, E.; DeBeer, S.; Wieghardt, K.; Chirik, P. J. *J. Am. Chem. Soc.* **2011**, *133*, 17353−17369.
(29) Bart, S. C.; Lobkovsky, E.; Bill, E.; Chirik, P. J. *J. Am. Chem. Soc.* **2006**, *128*, 5302−5303.
(30) Cowley, R. E.; Eckert, N. A.; Vaddadi, S.; Figg, T. M.; Cundari, T. R.; Holland, P. L. *J. Am. Chem. Soc.* **2011**, *133*, 9796−9811.
(31) Cowley, R. E.; Holland, P. L. *Inorg. Chem.* **2012**, *51*, 8352−8361.
(32) Lansky, D. E.; Kosack, J. R.; Sarjeant, A. A. N.; Goldberg, D. P. *Inorg. Chem.* **2006**, *45*, 8477−8479.
(33) Eikey, R. A.; Khan, S. I.; Abu-Omar, M. M. *Angew. Chem., Int. Ed.* **2002**, *41*, 3592−3595.
(34) Mandimutsira, B. S.; Ramdhanie, B.; Todd, R. C.; Wang, H. L.; Zareba, A. A.; Czernuszewicz, R. S.; Goldberg, D. P. *J. Am. Chem. Soc.* **2002**, *124*, 15170−15171.
(35) Lansky, D. E.; Mandimutsira, B.; Ramdhanie, B.; Clausén, M.; Penner-Hahn, J.; Zvyagin, S. A.; Telser, J.; Krzystek, J.; Zhan, R. Q.; Ou, Z. P.; Kadish, K. M.; Zakharov, L.; Rheingold, A. L.; Goldberg, D. P. *Inorg. Chem.* **2005**, *44*, 4485−4498.
(36) Prokop, K. A.; Goldberg, D. P. *J. Am. Chem. Soc.* **2012**, *134*, 8014−8017.
(37) Prokop, K. A.; de Visser, S. P.; Goldberg, D. P. *Angew. Chem., Int. Ed.* **2010**, *49*, 5091−5095.
(38) Prokop, K. A.; Neu, H. M.; de Visser, S. P.; Goldberg, D. P. *J. Am. Chem. Soc.* **2011**, *133*, 15874−15877.
(39) McGown, A. J.; Kerber, W. D.; Fujii, H.; Goldberg, D. P. *J. Am. Chem. Soc.* **2009**, *131*, 8040−8048.
(40) Cho, K.; Leeladee, P.; McGown, A. J.; DeBeer, S.; Goldberg, D. P. *J. Am. Chem. Soc.* **2012**, *134*, 7392−7399.
(41) Simkhovich, L.; Gross, Z. *Tetrahedron Lett.* **2001**, *42*, 8089−8092.
(42) Kerber, W. D.; Ramdhanie, B.; Goldberg, D. P. *Angew. Chem., Int. Ed.* **2007**, *46*, 3718−3721.
(43) Ramdhanie, B.; Stern, C. L.; Goldberg, D. P. *J. Am. Chem. Soc.* **2001**, *123*, 9447−9448.
(44) Aresta, M.; Nobile, C. F.; Petruzzelli, D. *Inorg. Chem.* **1977**, *16*, 1817−1818.
(45) Bittner, S.; Assaf, Y.; Krief, P.; Pomerantz, M.; Ziemnicka, B. T.; Smith, C. G. *J. Org. Chem.* **1985**, *50*, 1712−1718.
(46) Davidson, M. G.; Goeta, A. E.; Howard, J. A. K.; Lehmann, C. W.; McIntyre, G. M.; Price, R. D. *J. Organomet. Chem.* **1998**, *550*, 449−452.

(47) Kumar, D.; Karamzadeh, B.; Sastry, G. N.; de Visser, S. P. *J. Am. Chem. Soc.* **2010**, *132*, 7656−7667.
(48) Becke, A. D. *J. Chem. Phys.* **1993**, *98*, 5648−5652.
(49) Lee, C. T.; Yang, W. T.; Parr, R. G. *Phys. Rev. B* **1988**, *37*, 785−789.
(50) *Jaguar, version 7.9*; Schrodinger, LLC: New York, 2011.
(51) Frisch, M. J.; et al. *Gaussian 03, revision C.02*; Gaussian, Inc.: Wallingford, CT, 2004. See Supporting Information.
(52) Hay, P. J.; Wadt, W. R. *J. Chem. Phys.* **1985**, *82*, 270−283.
(53) de Visser, S. P. *J. Am. Chem. Soc.* **2010**, *132*, 1087−1097.
(54) Neese, F. *ORCA—An Ab Initio, DFT and Semiempirical SCF-MO Package, Version 2.9*; Bonn, Germany, 2009.
(55) Neese, F. *Inorg. Chim. Acta* **2002**, *337*, 181−192.
(56) Sinnecker, S.; Svensen, N.; Barr, E. W.; Ye, S.; Bollinger, J. M., Jr.; Neese, F.; Krebs, C. *J. Am. Chem. Soc.* **2007**, *129*, 6168−6179.
(57) Karamzadeh, B.; Kumar, D.; Sastry, G. N.; de Visser, S. P. *J. Phys. Chem. A* **2010**, *114*, 13234−13243.
(58) Betley, T. A.; Peters, J. C. *J. Am. Chem. Soc.* **2004**, *126*, 6252−6254.
(59) Scepaniak, J. J.; Fulton, M. D.; Bontchev, R. P.; Duesler, E. N.; Kirk, M. L.; Smith, J. M. *J. Am. Chem. Soc.* **2008**, *130*, 10515−15017.
(60) Mankad, N. P.; Muller, P.; Peters, J. C. *J. Am. Chem. Soc.* **2010**, *132*, 4083−4085.
(61) Abu-Omar, M. M.; Shields, C. E.; Edwards, N. Y.; Eikey, R. A. *Angew. Chem., Int. Ed.* **2005**, *44*, 6203−6207.
(62) Fructos, M. R.; Trofimenko, S.; Diaz-Requejo, M. M.; Perez, P. J. *J. Am. Chem. Soc.* **2006**, *128*, 11784−11791.
(63) Fantauzzi, S.; Caselli, A.; Gallo, E. *Dalton Trans.* **2009**, 5434−5443.
(64) Vyas, R.; Gao, G. Y.; Harden, J. D.; Zhang, X. P. *Org. Lett.* **2004**, *6*, 1907−1910.
(65) Harden, J. D.; Ruppel, J. V.; Gao, G. Y.; Zhang, X. P. *Chem. Commun.* **2007**, 4644−4646.
(66) Edwards, N. Y.; Eikey, R. A.; Loring, M. I.; Abu-Omar, M. M. *Inorg. Chem.* **2005**, *44*, 3700−3708.
(67) Bennett, B. K.; Saganic, E.; Lovell, S.; Kaminsky, W.; Samuel, A.; Mayer, J. M. *Inorg. Chem.* **2003**, *42*, 4127−4131.
(68) Cai, S.; Walker, F. A.; Licoccia, S. *Inorg. Chem.* **2000**, *39*, 3466−3474.
(69) Walker, F. A.; Licoccia, S.; Paolesse, R. *J. Inorg. Biochem.* **2006**, *100*, 810−837.
(70) Zakharieva, O.; Schünemann, V.; Gerdan, M.; Licoccia, S.; Cai, S.; Walker, F. A.; Trautwein, A. X. *J. Am. Chem. Soc.* **2002**, *124*, 6636−6648.
(71) Schwalbe, M.; Dogutan, D. K.; Stoian, S. A.; Teets, T. S.; Nocera, D. G. *Inorg. Chem.* **2011**, *50*, 1368−1377.
(72) Amusa, A.; Debrunner, P.; Frauenfe, H.; Münck, E.; DePasqua, G. *J. Phys. C* **1974**, *7*, 1881−1891.
(73) Teschner, T.; Yatsunyk, L.; Schunemann, V.; Paulsen, H.; Winkler, H.; Hu, C. J.; Scheidt, W. R.; Walker, F. A.; Trautwein, A. X. *J. Am. Chem. Soc.* **2006**, *128*, 1379−1389.
(74) Simonneaux, G.; Schunemann, V.; Morice, C.; Carel, L.; Toupet, L.; Winkler, H.; Trautwein, A. X.; Walker, F. A. *J. Am. Chem. Soc.* **2000**, *122*, 4366−4377.
(75) Kurahashi, S.; Ikeue, T.; Sugimori, T.; Takahashi, M.; Mikuriya, M.; Handa, M.; Ikezaki, A.; Nakamura, M. *J. Porphyrins Phthalocyanines* **2012**, *16*, 518−529.
(76) Gütlich, P.; Bill, E.; Trautwein, A. X. *Mössbauer Spectroscopy and Transition Metal Chemistry: Fundamentals and Applications*; Springer-Verlag: Berlin, 2011.
(77) Kostka, K. L.; Fox, B. G.; Hendrich, M. P.; Collins, T. J.; Rickard, C. E. F.; Wright, L. J.; Münck, E. *J. Am. Chem. Soc.* **1993**, *115*, 6746−6757.
(78) Jaccob, M.; Rajaraman, G. *Dalton Trans.* **2012**, *41*, 10430−10439.
(79) de Visser, S. P. *J. Am. Chem. Soc.* **2006**, *128*, 15809−15818.
(80) *Iron-Containing Enzymes: Versatile Catalysts of Hydroxylation Reactions in Nature*; de Visser, S. P., Kumar, D., Eds.; Royal Society of Chemistry Publishing: Cambridge, U.K., 2011.
(81) Stephens, J. C.; Khan, M. A.; Houser, R. P. *Inorg. Chem.* **2001**, *40*, 5064−5065.
(82) Chen, G.; Man, W. L.; Yiu, S. M.; Wong, T. W.; Szeto, L.; Wong, W. T.; Lau, T. C. *Dalton Trans.* **2011**, *40*, 1938−1944.
(83) Gröb, T.; Geiseler, G.; Harms, K.; Greiner, A.; Dehnicke, K. *Z. Anorg. Allg. Chem.* **2002**, *628*, 217−221.
(84) Schrumpf, F.; Roesky, H. W.; Noltemeyer, M. *Z. Naturforsch., B* **1990**, *45*, 1600−1602.
(85) Tomi, F.; Wah, H. L. K.; Postel, M. *New J. Chem.* **1988**, *12*, 289−292.
(86) Ding, Z. R.; Bhattacharya, S.; Mccusker, J. K.; Hagen, P. M.; Hendrickson, D. N.; Pierpont, C. G. *Inorg. Chem.* **1992**, *31*, 870−877.
(87) Chekhlov, A. N. *Russ. J. Inorg. Chem.* **2005**, *50*, 1207−1211.
(88) Atkinson, F. L.; Blackwell, H. E.; Brown, N. C.; Connelly, N. G.; Crossley, J. G.; Orpen, A. G.; Rieger, A. L.; Rieger, P. H. *J. Chem. Soc., Dalton. Trans.* **1996**, 3491−3502.
(89) Olejnik, Z.; Lis, T.; Ondrejkovicova, I. *Acta Crystallogr., Sect. C* **1995**, *51*, 2246−2249.
(90) Scepaniak, J. J.; Harris, T. D.; Vogel, C. S.; Sutter, J.; Meyer, K.; Smith, J. M. *J. Am. Chem. Soc.* **2011**, *133*, 3824−3827.